ARL 65-73
APRIL 1965

Aerospace Research Laboratories

LAMINAR MIXING AND HEAT TRANSFER PHENOMENA BETWEEN A PARTIALLY IONIZED GAS AND A GASEOUS COOLANT

JERRY GREY
PETER M. WILLIAMS
DAVID B. FRADKIN
PAUL F. JACOBS
MARTIN P. SHERMAN
PRINCETON UNIVERSITY
PRINCETON, NEW JERSEY

OFFICE OF AEROSPACE RESEARCH
United States Air Force

NOTICES

When Government drawings, specifications, or other data are used for any purpose other than in connection with a definitely related Government procurement operation, the United States Government thereby incurs no responsibility nor any obligation whatsoever; and the fact that the Government may have formulated, furnished, or in any way supplied the said drawings, specifications, or other data, is not to be regarded by implication or otherwise as in any manner licensing the holder or any other person or corporation, or conveying any rights or permission to manufacture, use, or sell any patented invention that may in any way be related thereto.

- - - - - - - - -

Qualified requesters may obtain copies of this report from the Defense Documentation Center, (DDC), Cameron Station, Alexandria, Virginia.

- - - - - - - - -

This report has been released to the Office of Technical Services, U. S. Department of Commerce, Washington 25, D. C. for sale to the general public.

- - - - - - - - -

Copies of ARL Technical Documentary Reports should not be returned to Aerospace Research Laboratories unless return is required by security considerations, contractual obligations or notices on a specified document.

400 - May 1965 - 448-39-830

BLANK PAGE

ARL 65-73

LAMINAR MIXING AND HEAT TRANSFER PHENOMENA BETWEEN A PARTIALLY IONIZED GAS AND A GASEOUS COOLANT

JERRY GREY
PETER M. WILLIAMS
DAVID B. FRADKIN
PAUL F. JACOBS
MARTIN P. SHERMAN

PRINCETON UNIVERSITY
PRINCETON, NEW JERSEY

APRIL 1965

Contract AF 33(657)-9962
Project 7063
Task 7063-01

AEROSPACE RESEARCH LABORATORIES
OFFICE OF AEROSPACE RESEARCH
UNITED STATES AIR FORCE
WRIGHT-PATTERSON AIR FORCE BASE, OHIO

FOREWORD

This is an Interim Documentary Report of research performed by the Department of Aerospace and Mechanical Sciences, Princeton University, under Contract AF 33(657)9962. Although the period covered by this report extends from 1 October 1962 through 31 August 1964, the first year's work was described in detail by an Interim Documentary Report, ARL 63-237, issued in December, 1963 (see Reference 1). The present report, therefore, emphasizes the period from 1 October 1963 through 31 August 1964, with Reference 1 serving to provide some of the pertinent background. Other specific areas have also been reported separately, and are referenced at appropriate places in the text.

The research program described in this report made use of computer facilities supported in part by National Science Foundation Grant NSF-GP579 to Princeton University.

ABSTRACT

Mixing and heat transfer characteristics of a laminar subsonic argon arcjet issuing into a stagnant atmosphere of room-temperature helium have been investigated by a combined analytical-experimental approach. Typical initial conditions of the one-centimeter-diameter jet were 20,000°R at one atmosphere, providing about 7% ionization of the argon.

The analysis was based on classical continuum theory utilizing the boundary-layer approximation. Electron-heavy particle equilibrium was assumed, based on prior estimates for the specific conditions investigated, and the transport properties necessary for the solution were computed by a modified Chapman-Enskog method.

Detailed local measurements of the mixing field were made up to five inches (about 12 jet diameters) downstream of the arcjet nozzle exit, utilizing a previously-developed calorimetric sampling probe capable of measuring local values of enthalpy, stagnation pressure, and gas composition.

Good correlation between theory and experiment was observed. Decay of the hot laminar jet was dominated by the inflow of helium, the observed effects of ion recombination, radiation, and jet dispersion being minor or negligible. As indicated by the theory, this behavior resulted from the high specific heat and high diffusion coefficients of helium at arcjet temperatures.

Although the departure from equilibrium between the electrons and the heavy particles was estimated to be sufficiently small when considering the overall mixing process, it was shown

analytically that this equilibrium probably did not exist in the regions of highest temperature gradient. It was, therefore, decided to explore the nature of this departure in the high-density (one atmosphere) collision-dominated, partly-ionized gas by the use of a cooled electrostatic probe. The theory for such a probe has been formulated, and it appears to provide the capability for measuring both electron concentrations and electron temperatures. This theory was confirmed in a rather approximate manner by a rough experimental check, and detailed studies of this technique will therefore be instituted in a subsequent research program.

TABLE OF CONTENTS

LIST OF ILLUSTRATIONS

BLANK PAGE

I. INTRODUCTION

Studies of arcjet mixing and heat transfer have been under way at Princeton since 1958, with the objective of establishing a comprehensive and generalized model for the mixing of a partially ionized gas jet with a gaseous coolant. Past work initiated the study of a turbulent arcjet (2)* and the study of arcjet radiation heat transfer (3). During the course of this work a calorimetric probe for measuring temperature, velocity, and composition in the hot core and the mixing region was developed for use at temperatures of the order of 25,000°F (4). A total radiation probe for use up to this temperature range was also developed (5). An integral analysis of the turbulent mixing was performed and the results agreed well with the data (6).

Recent work has been addressed to the case of an initially laminar arcjet, since laminar flows are amenable to theoretical analysis. During this investigation, refinements were made in the instrumentation (1), a study of electron-heavy particle equilibrium was performed (7), and computations of laminar transport properties (8) were made. The current experimental work reported herein deals mostly with free-jet laminar mixing, although pertinent results of a similar bounded mixing study, performed for NASA (9), are included.

Continued work is planned which will exploit the information and techniques now available. Studies investigating supersonic

*Numbers in parentheses indicate References listed on page 72.

Manuscript released by the authors November 1964 for publication as a ARL technical report.

jets, ambient gases other than helium, and the effects of externally-imposed electric and magnetic fields are planned. In addition, NASA-supported work will investigate in detail the effects of the arcjet-to-coolant velocity ratio over a wide range and the effects of the scale of initial turbulence of both the arcjet and coolant streams.

While the fundamental objective of the program is to provide a basic understanding of the physical processes, it is also expected that theoretical and experimental results can be correlated into generalized relationships involving traditional engineering design parameters so that they will be useful in certain practical applications. Reference (1) indicated, in some detail, potential applications to the gaseous-core nuclear rocket, to thrust augmentation systems, and to film-cooling of chambers for extreme-energy propulsion systems. The advent of the high specific impulse arcjet thruster (10) adds particular interest to the thrust augmentation application.

II. LAMINAR MIXING THEORY AND EXPERIMENT

A. THEORETICAL ANALYSIS

1. Introduction

A technique for computing the mixing and heat transfer of a free argon arcjet to an atmosphere of cold helium has been developed during the course of the present research. Comparisons of experimental and theoretical data, given in Section II-C, are

satisfactory,and the theoretical model presented here is believed to be representative of the dominant processes involved. This model uses a boundary-layer type analysis in which the species conservation equations and transport properties include the effects of ionization. The model assumes effective equilibrium between electrons and heavy particles. Computation of the transport properties and estimation of the approach to equilibrium constituted major theoretical efforts, the results of which are summarized in Reference (1). This work has been reported in detail in Reference (11). Reference (11) also contains a complete exposition of the boundary layer analysis, including the numerical techniques used to integrate and solve the equations on a IBM 7094 computor. A portion of Reference (11) dealing with the development of the boundary layer analysis is summarized in the present report,illustrating the important working assumptions necessary for the theoretical model. This model represents the basic contribution to the theory of ionized gas mixing. Other aspects of the overall theoretical problem appear in Reference (11).

2. History of Laminar Jet Mixing

The boundary layer approximation was first advanced by Prandtl early in the twentieth century to deal with the flow of a slightly viscous fluid over a surface whose principal effect on the flow field was confined to a small region adjacent to the surface. The approximations of boundary layer theory

have been applied to the mixing of fluid streams in several geometries: (a) the mixing of two semi-infinite streams, (b) the mixing of a two-dimensional jet into an infinite stream, (c) the mixing of an axisymmetric jet into a infinite stream, and (d) similar mixing situations, but confined within ducts. The following discussion is limited to laminar mixing, and concentrates on the case of axisymmetric jet mixing into a infinite stream. The uniqueness of the present treatment lies principally in the nature of the gas, which is at sufficiently high temperatures to produce a significant degree of ionization.

The single analytical technique which did not utilize the boundary layer approximation was that described by Squire (12), who found a class of similar solutions to the incompressible Navier-Stokes equations in spherical coordinates with azimuthal symmetry. One subgroup of these solutions corresponds to the flow of a round laminar jet far from the nozzle. The application of similar solutions, which are valid only far from the orifice, was also considered in analytical studies of the incompressible two-dimensional jet by Schlichting (13) and Bickley (14), and the incompressible axisymmetric jet by Schlichting (13).

For compressible jets or heated jets, however, the picture becomes more complex. Various solutions have been published using a number of approximations; e.g., the dependence of the transport properties on temperature. This was done for the two-dimensional jet by Toose (15), for the axisymmetric jet by

Pack (16), and for the mixing of two different types of incompressible gases in both plane and axisymmetric jets by Crane and Pack (17). All of these analyses required the use of many assumptions in order to be able to provide solutions.

Of more immediate interest is the mixing of jets at near and moderate distances from the nozzle. This is a problem for which there have been very few analytic solutions, and even these required the use of very restrictive assumptions. Most noteworthy are those of Kleinstein (18) and Pai (19,20).

In the even more complex problem of chemically-reacting flows, the work of Marble and Adamson (21) and Cheng and Kovitz (22) on the mixing of a compressible cool stream with a hot "burnt-gas" stream, together with that of Kovitz (23) on the mixing of dissociated streams, are illustrations of the use of simplifying assumptions to obtain equations which can be handled analytically.

In recent years, with the availability of high-speed digital computers, the popularity of numerical solutions for jet mixing problems has increased; e.g., the work of Pai (19,20). These numerical developments can also utilize similarities to a limited extent. Finite difference methods, particularly implicit finite difference methods, are increasing in favor as the computing times necessary for application of these methods has been reduced. An illustration of the use of numerical techniques in the solution of a jet mixing problem

is given by Weinstein (24).

3. Development of the Fluid Mechanical Equations of Mixing

In this sub-section the pertinent fluid mechanical equations are developed. When the general equations are expressed in a cylindrical coordinate system, the problem becomes two-dimensional as a result of the assumptions of axial symmetry and zero flux in the angular direction. The boundary layer assumptions are used to simplify the equations, which are then converted to a more suitable form by the use of the Von Mises transformation. The resulting differential equations are approximated by difference equations which may then be solved on a high-speed digital computer.

1. Assumptions

1. The flow is in local thermodynamic equilibrium.
2. Only four species need be considered explicitly: (a) argon atoms in the ground state, (b) singly ionized argon ions in the ground state, (c) helium atoms, (d) electrons.
3. The flow is steady.
4. The flow is laminar.
5. The flow is axisymmetric, with no currents in the angular direction.
6. The pressure is constant.
7. The boundary layer approximation is valid.
8. The mixture obeys the perfect gas laws (see Appendix for nomenclature):

$$p_i^* = n_i^* k T^*, \qquad p = \sum p_i^* = n^* k T^*$$

9. The gas is optically thin.

10. The diffusion currents of the ions and electrons are equal (ambipolar diffusion).

11. There are no externally-applied electric or magnetic fields.

12. Gravity forces are neglected.

The validity of the assumption of local thermodynamic equilibrium is discussed in some detail in References 1 and 11. The mole fractions of the doubly-ionized argon and singly-ionized helium are so small that they may be ignored in computing the thermodynamic and transport properties, and are not explicitly considered in the analysis. The contribution of excited electronic states will be largest at about 12,500°K. At 12,500°K and 1 atmosphere pressure, the electronic partition function of the argon atom is 1.009. Hence the electronically-excited mole fraction is less than 10^{-2}, and the electronic contribution to the enthalpy is about 2.5%. This small electronic effect is the result of comparable contributions from a large number of electronic levels. At lower temperatures the electronic mole fraction will decrease, whereas at higher temperatures ionization increases rapidly. Thus, the energy contribution of the excited electronic states is not considered in the analysis. Of course, the electronically excited levels do play an important role in the kinetics. The evidence obtained from ultra-high-speed and schlieren photographs (Figs. 1, 2), together with the calorimetric probe data, indicates that the plasmajet exhaust can be described reasonably well by the assumptions of laminar,

steady, axisymmetric flow. In the low subsonic free jet used in the experiment, pressure gradients are small and can be neglected (27). Although the boundary layer assumption is not valid adjacent to the nozzle edge, it becomes quite satisfactory further downstream, as discussed in Reference 11 . For a discussion of the validity of the perfect-gas approximation in partially-ionized gases see Reference 28 . The perfect gas law is shown to be good under the conditions of interest. The radiation characteristics of the partially-ionized argon are discussed in Reference 3 . Ambipolar diffusion implies that the plasma is nearly neutral, or "quasi-neutral", and that there are no net electric currents. The validity of this assumption cannot be proven; however, it does seem that the assumption is reasonable except at the cold outer boundaries, because the Debye length is much smaller than the characteristic dimensions of the experiment for the significant mole fractions of charged particles. The Debye length is given by

$$h = \sqrt{\frac{kT}{4\pi e^2 N_e}} = 6.9 \sqrt{\frac{T}{N_e}} \quad \text{cm.}$$

and even at 5000°K is only of the order of 10^{-3}cm.

2. The Number and Coupling of the Equations

In a fluid mechanical system of "n" species for which there is an equation of state, and in which there are chemical reactions, mass motions, and temperature gradients, there are in general (n + 5) equations to consider: an overall continuity

equation, an equation of state, and (n - 1) species continuity equations (the n^{th} species continuity equation is not independent, since it can be derived from the overall continuity equation and the n - 1 species continuity equations). For a four-component system, therefore, there are nine equations.

The basic assumptions given above reduce this intractable general problem to the far simpler case of only three simultaneous parabolic partial differential equations. Assumptions 1, 2, and 10 imply that the electron and ion concentrations are equal, and that the relative concentrations of argon ions to argon neutrals is given by the equilibrium relation for partly-ionized argon. Thus the composition of the four-species gas is determined if the concentration of only one species is known, together with the temperature and pressure. Only one species continuity equation now remains independent; in the present analysis, the helium continuity equation is used, with the helium mole fraction taken as the principal composition variable. The assumptions of axial symmetry and the boundary assumption leave the axial momentum equation as the only momentum equation still relevant. The perfect gas equation of state is easily incorporated into the other equations.

By use of the Von Mises transformation, the overall continuity equation is identically satisfied, and the radial component of velocity is no longer explicitly considered. Hence, the only equations remaining are (1) the axial momentum

equation, (2) the helium continuity equation, and (3) the energy equation. The main dependent variables are (1) the axial velocity, (2) the helium mole fraction, and (3) the temperature.

The helium diffusion equation and the energy equation are intimately coupled through the dependence of the thermodynamic properties, the transport properties, and the radiation on the temperature and the helium mole fraction. In contrast, the momentum equation is coupled to the other two equations only through the presence of the product $\rho\mu$. In many analyses of simpler mixing problems this product is assumed constant so that the momentum equation may be solved independently. In the present problem, unfortunately, none of the various stratagems generally used to uncouple the momentum equation are justifiable.

4. Preliminary Definitions

In this sub-section the definitions of the basic fluid mechanical quantities used in this analysis are presented, together with some simple basic relations. The definitions and much of the notation are conventional (25,26,21,23). Nomenclature appears in the **Appendix.**

The partial density ρ_i^* of a species i, and the total density ρ^*, are defined by

$$\rho_i^* = m_i \dot{m}_i^* = m_i m^* x_i \qquad \text{II-(1)}$$

$$\rho^* = \sum \rho_i^* = m^* \sum m_i x_i \qquad \text{II-(2)}$$

For our system,

$$\rho = m_A m_A^* + m_N m_N^* + m_I m_I^* + m_e m_e^* \qquad \text{II-(3)}$$
$$= m_A m^* (x_A + R x_N + x_e)$$
$$\equiv m_A m^* \bar{X} \qquad R \equiv \frac{m_N}{m_A} = 0.1002$$
$$x_I = x_e$$

The velocity $\vec{C}_o^*$ of the center of gravity of a fluid element, the mass average velocity, is the macroscopically observed fluid velocity.

$$\vec{C}_o^* = \frac{1}{\rho^*} \sum \rho_i \overline{\vec{C}_i^*} \qquad \text{II-(5)}$$

The diffusion velocity of the i^{th} species is defined as the average velocity of that species relative to the mass average velocity:

$$\vec{C}_i^* \equiv \overline{\vec{C}_i^*} - \vec{C}_o^* \qquad \text{II-(6)}$$

From the above we easily obtain

$$\sum m_i m_i^* \vec{C}_i^* = m^* \sum m_i x_i \vec{C}_i^* = 0 \qquad \text{II-(7)}$$

The rate of production K_i^* of a species i per unit volume by chemical reaction is subject to the constraint:

$$\sum m_i K_i^* = 0 \qquad \text{II-(8)}$$

For our system,

$$K_e^* = K_I^* = -K_A^*$$
$$K_N^* = 0 \qquad \text{II-(9)}$$

The pressure tensor is defined by:

$$\overline{\overline{P}}^* = \sum \overline{\overline{P}}_i^* = \sum m_i \int f_i \vec{c}_i^* \vec{c}_i^* \, d^3c = \sum m_i m_i \overline{\vec{c}_i \vec{c}_i} \qquad \text{II-(10)}$$

To the level of approximation of the Navier-Stokes equation, taking the dilatational coefficient of viscosity as zero, the pressure tensor is expressed in terms of macroscopic quantities in the form:

$$\overline{\overline{P}} = p^* \overline{\overline{I}} - 2\mu \overline{\overline{S}}$$
$$\overline{\overline{S}} = \frac{1}{2}\left[\vec{\nabla}\vec{c}_o^* + (\vec{\nabla}\vec{c}_o^*)^{\text{TRANSPOSE}} - \frac{2}{3}\vec{\nabla}\cdot\vec{c}_o^* \overline{\overline{I}}\right] \qquad \text{II-(11)}$$

The perfect gas assumption requires

$$\frac{\partial h_i^*}{\partial s} = \left(\frac{\partial h_i^*}{\partial T^*}\right)\frac{\partial T^*}{\partial s} + \left(\frac{\partial h_i^*}{\partial p}\right)\frac{\partial p^*}{\partial s}$$
$$= c_{p_i}^* \frac{\partial T^*}{\partial s} \qquad \text{II-(12)}$$

where S is some symbolic variable. In the absence of rotational and vibration energy and the neglect of electronic excitation, the specific heat of the various species will be constant. The convention used is that the ionization energy resides in the electrons. The species enthalpies and specific heats are

as follows:

$$h_j^* = \frac{5}{2}\frac{kT^*}{m_j} \; ; \quad c_{p_j} = \frac{5}{2}\frac{k}{m_j} \qquad j = A, M, I$$

$$h_e^* = \frac{5}{2}\frac{kT^*}{m_e} + \frac{I^*}{m_e} \; ; \quad c_{p_e} = \frac{5}{2}\frac{k}{m_e} \qquad \text{II-(13)}$$

where I is the ionization energy per electron (15.75 E.V. or 25.2×10^{-12} erg). The total enthalpy and the total specific heat are:

$$h^* = \frac{1}{\rho^*}\sum \rho_i^* h_i^* \qquad \text{II-(14)}$$

$$c_p^* = \frac{1}{\rho^*}\sum \rho_i^* c_{p_i}^* \qquad \text{II-(15)}$$

Note that the total specific heat as defined here is not the constant-pressure derivative of the enthalpy with respect to temperature, but rather:

$$\left(\frac{\partial h^*}{\partial T}\right)_p = c_p^* + \sum h_i \left(\frac{\partial w_i}{\partial T^*}\right)_p \qquad \text{II-(16)}$$

where w_i = mass fraction of species i

The diffusion velocities are expressed in terms of diffusion coefficients and thermal diffusion coefficients:

$$\vec{c}_i^* = \frac{1}{x_i M}\sum M_i D_{ij} \vec{d}_j - \frac{M_i D_i^{T^*}}{\rho x_i M_i}\vec{\nabla} \ln T^* \qquad \text{II-(17)}$$

$$\vec{d}_j = \vec{\nabla} x_j + x_j \left(1 - \frac{M_j}{M}\right) \vec{\nabla} \ln p^* - \frac{x_j}{RT^*} \cdot \left[\vec{F}_j^* - \frac{M_j}{M} \sum_k x_k \vec{F}_k^*\right] \qquad \text{II-(18)}$$

where

$$M \equiv \sum M_j x_j = M_k \bar{x} \qquad \text{II-(19)}$$

Since the only body force considered is the self-induced electric field caused by ambipolar diffusion,

$$\vec{F}_k^* = \vec{\mathcal{E}} e z_k \qquad \text{II-(20)}$$

so

$$\vec{F}_A^* = \vec{F}_M^* = 0$$
$$\vec{F}_\Sigma^* = \vec{\mathcal{E}} e = -\vec{F}_e^*$$
$$\sum \vec{F}_k^* x_k = 0$$

With the assumption of constant pressure, the "diffusive forces" $\vec{d}_j$ reduce to:

$$\vec{d}_j = \vec{\nabla} x_j - \frac{e x_j z_j}{RT^*} \vec{\mathcal{E}} \qquad \text{II-(21)}$$

The electric field can be eliminated from explicit consideration by the use of effective diffusion coefficients as discussed in Reference 11.

5. The General Equations

The general fluid mechanical equations pertinent to

the problem are

Overall continuity

$$\frac{\partial \rho^*}{\partial t^*} + \vec{\nabla} \cdot (\vec{c}_o^* \rho^*) = 0 \qquad \text{II-(21)}$$

Momentum

$$\frac{\partial \vec{c}_o^*}{\partial t^*} + \vec{c}_o^* \cdot \vec{\nabla} \vec{c}_o^* = \frac{-1}{\rho^*} \vec{\nabla} \cdot \vec{\vec{P}}^* + \sum m_i^* \vec{F}_i^* \qquad \text{II-(22)}$$

Helium continuity

$$\frac{\partial}{\partial t^*}\left(m^* x_n\right) + \vec{\nabla} \cdot \left\{ m^* x_n \left[\vec{c}_o^* + \vec{c}_n^* \right] \right\} = K_n^* = 0 \qquad \text{II-(23)}$$

Energy

$$\rho \frac{\partial U^*}{\partial t^*} + \rho \vec{c}_o^* \cdot \vec{\nabla} U^* = -\vec{\nabla} \cdot \vec{q}^* - \vec{\vec{P}}^* : \vec{\nabla} \vec{c}_o^* + \sum m_i^* \vec{c}_i^* \cdot \vec{F}_i^* - \vec{\nabla} \cdot \vec{q}_{rad}^* \qquad \text{II-(24)}$$

where the energy flux vector $\vec{q}^*$ is given by:

$$\vec{q}^* = -\lambda^* \vec{\nabla} T^* + \sum \rho_i^* \vec{c}_i^* h_i^* + m^* k T^* \sum \frac{D_i^T \vec{d}_i^*}{m_i^* m_i} \qquad \text{II-(25)}$$

This can be transformed into the more convenient form (21,22),

$$\rho^* c_p^* \left\{ \frac{\partial T^*}{\partial t^*} + \vec{c}_o^* \cdot \vec{\nabla} T^* \right\} = \vec{\nabla} \cdot \lambda^* \vec{\nabla} T^* - \sum m_i m_i^* c_{p_i}^* \vec{c}_i^* \cdot \vec{\nabla} T^* - \sum m_i h_i^* X_i + \frac{\partial p^*}{\partial t} + \vec{c}_o^* \cdot \vec{\nabla} p^* - \vec{\nabla} \cdot \left[m^* k T^* \sum \frac{D_i^T d_i^*}{m_i^* m_i} + \vec{q}_{rad}^* \right] + \Phi \qquad \text{II-(26)}$$

State

$$p^* = m^* k T^*$$

Body Force Terms

Making use of the assumptions of neutrality and ambipolar diffusion, the body force terms in the momentum and the energy equation are zero:

$$\sum M_i^* \vec{F}_i^* - e\vec{E}(M_i^* - M_e^*) = 0 \qquad \text{II-(27)}$$

$$\sum M_i \vec{C}_i \cdot \vec{F}_i^* = e\vec{E} \cdot \left[M_i^* \vec{C}_i^* - M_e^* \vec{C}_e^* \right] = 0$$

We drop the unsteady terms and the pressure gradient terms by assumptions 3 and 8.

Radiation Terms

Using the assumption of an optically thin gas (verified by experiments described in Reference 3), the divergence of the radiant heat flux vector is the rate at which radiant energy is being emitted per unit volume, P_{rad}. Neglecting the weak explicit dependence on temperature, the radiation is taken to be proportional to the square of the electron density as discussed in Reference 11:

$$P_{rad} \sim (M_e^*)^2 \sim (M^* X_e)^2 \qquad \text{II-(28)}$$

Viscous Dissipation

The viscous dissipation Φ is neglected, since it will be quite small compared to the other terms at the low Mach numbers present in the flow.

Thermal Diffusion Effects

It is advantageous, although not essential, to be able to neglect the thermal diffusion effects. First we consider the effect of thermal diffusion on the diffusion velocity. At low temperatures the ionization can be neglected and we have (26):

$$\bar{C}_H^* - \bar{C}_A^* = \frac{-1}{X_A X_H} \alpha D_{AH}^* \left[\bar{\nabla} X_A - k(T) \nabla \ln T^* \right] \qquad \text{II-(29)}$$

where

$$k(T) = \frac{\rho^* D_H^*}{M^{*2} m_A m_H \alpha D_{AH}^*} \quad = \text{thermal diffusion ratio} \qquad \text{II-(30)}$$

A useful quantity is the thermal diffusion factor α, which is nearly constant for different composition ratios:

$$\alpha = \frac{k(T)}{X_A X_H} \qquad \text{II-(31)}$$

The value obtained at 5000°K, $X_H = 0.5$, is in close agreement with the value 0.33 given in Reference 29. Considering an extreme case, let:

$$\nabla X_A = \frac{1}{2} \qquad \nabla \ln T^* = 1$$

Then

$$\frac{k(T) \nabla \ln T^*}{\nabla X_A} = \frac{1}{6}$$

The effect of thermal diffusion in the extreme case is still

small, and may therefore be neglected. An analysis of the high-temperature case also led to the conclusion that thermal diffusion could be ignored.

The expression for the energy flux q is not the same as in (26). Hirschfelder uses a more complex expression in which the thermal diffusion coefficient term is broken up into a diffusive and a non-diffusive term:

$$q^* = -\lambda'^* \nabla T^* + \sum_i \rho_i^* c_i^* h_i^* + \frac{k_T^*}{m^*} \sum_i \frac{m_i^* D_i^{T*} (c_i^* - c_j^*)}{m_i \mathcal{D}_{ij}} \qquad \text{II-(32)}$$

$$\lambda'^* = \lambda^* - \frac{1}{2} R \sum_i \sum_{j \neq i} \frac{R T^* x_i x_j}{\rho^* \mathcal{D}_{ij}} \left[\frac{D_i^{T*}}{x_i m_i} - \frac{D_j^{T*}}{x_j m_j} \right]$$

For our purposes the form presented earlier is preferable. After some algebra we obtain:

$$m^* k_T^* \sum \frac{D_i^{T*} d_j^*}{m_j m_j} = R T^* \left[\frac{D_A^{T*} d_A^*}{x_A m_A} + \frac{D_N^{T*} d_N^*}{x_N m_N} + \frac{D_E^{T*} d_E^*}{x_E m_E} + \frac{D_e^{T*} d_e^*}{x_e m_e} \right] \qquad \text{II-(33)}$$

Two cases were considered. At low temperatures only the first two terms remain. Substituting reasonable values for d_A^* and ∇T^*, the thermal diffusion term should be less than 10% of the ordinary thermal conductivity term. At high temperatures the "diffusive driving forces" d_j^* for the electrons and the ions must include the effect of ambipolar diffusion. The result is to greatly reduce the electron term, the only term that could have been significant. The thermal diffusion coefficient term in the energy equation is therefore neglected.

Diffusive Term

Using Eq (II-13), Eq (II-9), the chemical production term of the energy equation becomes

$$\sum m_i^* h_i^* K_i^* = -\frac{5}{2} \lambda T^* K_A^* \left[1 + \frac{I^*}{5/2 \lambda T^*} \right] \qquad \text{II-(35)}$$

The helium continuity equation is put into a more satisfactory form by the following manipulations. Expanding Eq (II-23)

$$m^* \mu^* \frac{\partial X_A}{\partial x^*} + m^* v^* \frac{\partial X_A}{\partial r^*} + X_A \left[\frac{\partial}{\partial x^*}(m^* \mu^*) + \frac{1}{r^*} \frac{\partial}{\partial r^*}(r^* m^* v^*) \right] = \frac{-1}{r^*} \frac{\partial}{\partial r^*}(r^* m^* X_A V_A^*) \qquad \text{II-(36)}$$

Subtracting the overall continuity equation in the form

$$X_A \left[\frac{\partial}{\partial x^*}(m^* \mu^*) + \frac{1}{r^*} \frac{\partial}{\partial r^*}(r^* m^* v^*) \right] + \frac{X_A}{\bar{X}} \left[m^* \mu^* \frac{\partial \bar{X}}{\partial x^*} + m^* v^* \frac{\partial \bar{X}}{\partial r^*} \right] = 0 \qquad \text{II-(37)}$$

we obtain:

$$m^* \mu^* \left[\frac{\partial X_A}{\partial x^*} - \frac{X_A}{\bar{X}} \frac{\partial \bar{X}}{\partial x^*} \right] + m^* v^* \left[\frac{\partial X_A}{\partial r^*} - \frac{X_A}{\bar{X}} \frac{\partial \bar{X}}{\partial r^*} \right] = \frac{1}{r^*} \frac{\partial}{\partial r^*}(r^* m^* X_A V_A^*) \qquad \text{II-(38)}$$

In this form only mole fractions appear in the axial derivatives. Ultimately only axial derivatives of helium mole fraction will appear, together with those of the temperature and the velocity.

Consider the axial derivative of $\bar{X}$

$$\frac{\partial \bar{X}}{\partial x^*} = \frac{\partial X_A}{\partial x^*} + R\frac{\partial X_N}{\partial x^*} + \frac{\partial X_e}{\partial x^*}$$

$$= \frac{1}{2}\frac{\partial X_A}{\partial x^*} - \frac{1}{2}\left[1-2R\right]\frac{\partial X_N}{\partial x^*} \qquad \text{II-(39)}$$

$$= -\tfrac{1}{2}\left[1-2R-\frac{\partial X_A}{\partial X_N}\right]\frac{\partial X_N}{\partial x^*} + \frac{1}{2}\frac{\partial X_A}{\partial T^*}\frac{\partial T^*}{\partial x^*}$$

Making use of the assumptions just described the fluid mechanical equations become:

$$\frac{1}{r^*}\frac{\partial}{\partial r^*}\left(\rho^* N^* r^*\right) + \frac{\partial}{\partial x^*}\left(\rho^* u^*\right) = 0 \qquad \text{II-(40)}$$

$$\rho^* u^*\frac{\partial u^*}{\partial x^*} + \rho^* N^*\frac{\partial u^*}{\partial r^*} = \frac{1}{r^*}\frac{\partial}{\partial r^*}\left(r^*\mu^*\frac{\partial u^*}{\partial r^*}\right) \qquad \text{II-(41)}$$

$$m^* u^*\left[\frac{\partial X_N}{\partial x^*} + \frac{X_N}{2\bar{X}}\left\{\left(1-2R-\frac{\partial X_A}{\partial X_N}\right)\frac{\partial X_N}{\partial x^*} - \frac{\partial X_N}{\partial T^*}\frac{\partial T^*}{\partial x^*}\right\}\right]$$

$$+ m^* N^*\left[\frac{\partial X_N}{\partial r^*} + \frac{X_N}{2\bar{X}}\left\{\left(1-2R-\frac{\partial X_A}{\partial X_N}\right)\frac{\partial X_N}{\partial r^*} - \frac{\partial X_N}{\partial T^*}\frac{\partial T^*}{\partial r^*}\right\}\right] = \frac{1}{r^*}\frac{\partial}{\partial r^*}\left(r^* m^* X_N V_N^*\right)$$

II-(42)

$$\rho^* c_p^*\left[u^*\frac{\partial T^*}{\partial x^*} + N^*\frac{\partial T^*}{\partial r^*}\right] = \frac{1}{r^*}\frac{\partial}{\partial r^*}\left(r^*\lambda^*\frac{\partial T^*}{\partial r^*}\right) - P_{rad}^*$$

$$- \frac{\partial T^*}{\partial r^*}\cdot\frac{5}{2}k\sum m_i^* V_i^* \qquad \text{II-(43)}$$

$$+ \frac{5}{2}k_{(T)}^* K_A^*\left[1 + I^*/\frac{5}{2}kT^*\right]$$

At this time it is necessary to obtain a specific form for the net rate of production K^*_A of argon atoms by recombination. Using the assumption of local thermodynamic equilibrium, an expression is developed in Reference 11 which contains only fluid mechanical variables, thermodynamic

variables, and diffusion velocities. No information on the kinetics of the reaction appear. The result is

$$K_A^* = \frac{m_A^*}{\left[1 + x_A - x_H \frac{\partial x_A}{\partial x_H}\right]} \left[\left(\frac{\partial x_A}{\partial T}\right)\left(u^* \frac{\partial T^*}{\partial x^*} + v^* \frac{\partial T^*}{\partial r^*}\right)\right]$$

$$+ \frac{1}{r^*} \frac{\partial}{\partial r^*} \left[r^* m^* x_A V_A^*\right] \qquad \text{II-(44)}$$

$$+ \frac{(1-2R)\left[x_H \frac{\partial x_A}{\partial x_H} - x_A\right] - \frac{\partial x_A}{\partial x_H}}{\left(1 + x_A - x_H \frac{\partial x_A}{\partial x_H}\right)} \frac{1}{r^*} \frac{\partial}{\partial r^*} \left[r^* m^* x_H V_H^*\right]$$

Note that at low temperatures, where the ionization becomes negligible,

$$\frac{\partial x_A}{\partial T^*} \longrightarrow 0$$

$$\frac{\partial x_A}{\partial x_H} \longrightarrow -1 \qquad \text{II-(45)}$$

$$R V_H^* - V_A^* \longrightarrow 0$$

Hence by inspection it can be seen that, as would be expected,

$$K_A^* \longrightarrow 0 \qquad \text{II-(46)}$$

The diffusion velocities can be put into a much more satisfactory form. Consider the helium diffusion velocity:

$$V_H^* = \frac{1}{x_H \bar{x}} \left[D_{HA}^* \frac{\partial x_A}{\partial r^*} + R D_{HH}^* \frac{\partial x_H}{\partial r^*} + D_{H^+}^* \frac{\partial x_{z^+}}{\partial r^*} + \frac{m_e}{m_A} D_{He}^* \frac{\partial x_e}{\partial r^*}\right] \text{II-(47)}$$

Making use of Eqs (II-4) and (II-7), and the identity

$$\frac{m_e}{m_A} D_{He}^* = D_{Hz} \qquad \text{II-(48)}$$

we obtain

$$V_N^* = \frac{1}{X_N \bar{X}} \left[(R D_{NN}^* - D_{NA}^*) \frac{\partial X_N}{\partial r^*} + 2 (D_{Ne}^* - D_{NA}^*) \frac{\partial X_e}{\partial r^*} \right] \quad \text{II-(49)}$$

Likewise:

$$V_A^* = \frac{1}{X_A \bar{X}} \left[(R D_{AN}^* - D_{AA}^*) \frac{\partial X_N}{\partial r^*} + 2 (D_{Ae}^* - D_{AA}^*) \frac{\partial X_e}{\partial r^*} \right] \quad \text{II-(50)}$$

The latter forms are greatly preferable to the earlier ones. The diffusion coefficients will always occur in the four combinations:

$$\textcircled{1} \quad (R D_{NN}^* - D_{NA}^*) \qquad \textcircled{3} \quad (R D_{AN}^* - D_{AA}^*) \qquad \text{II-(51)}$$

$$\textcircled{2} \quad 2 (D_{Ne}^* - D_{NA}^*) \qquad \textcircled{4} \quad 2 (D_{Ae}^* - D_{AA}^*)$$

necessitating the use of four rather than eight diffusive coefficients. There is an additional benefit in the use of the diffusion coefficients combined in the four groups shown above. At low temperatures the second and fourth groups are of no importance, since they occur in terms which go to zero as the ionization vanishes. The effective diffusion coefficients appearing in the first and third groups do not approach the values of these terms using ordinary diffusion coefficients. Hence by the use of diffusion coefficients only in these groupings, a smooth transition is achieved from the low-temperature two-component no-ionization case to the high-temperature four-species partly-ionized case.

6. Nondimensionalization

The equations are nondimensionalized by the use of various reference quantities:

$$r = \frac{r^*}{r_o} \qquad x = \frac{x^*}{r_o} \qquad \mu = \frac{\mu^*}{\mu_o} \qquad \nu = \frac{\nu^*}{\mu_o} \qquad \rho = \frac{\rho^*}{\rho_o} \qquad m = \frac{m^*}{m_o}$$

$$c_p = c_p^*/c_{p_o} \qquad p = p^*/p_o \qquad \mu = \mu^*/\mu_o \qquad D_{ij} = D_{ij}^*/D_o$$

$$T = T^*/T_o \qquad I = I^*/\tfrac{5}{2} h T_o \qquad \lambda = \lambda^*/\lambda_o \qquad P_{rad} = \frac{P_{rad}^*}{P_{rad_o}}$$

The characteristic length used in this analysis is the radius of the nozzle. The other reference quantities, identified by the subscript zero, are values of the properties at the midpoint of the nozzle exit plane. Note that:

$$c_{p_o} = \tfrac{5}{2} h \frac{m_o}{\rho_o} \qquad \rho_o = m_o m_o \qquad \text{II-(53)}$$

and

$$\rho c_p = m \qquad \text{II-(54)}$$

The nondimensionalized perfect gas law for constant pressure reduces to the simple relation:

$$m = 1/T \qquad \text{II-(55)}$$

Nondimensionalization of the equations will introduce the following nondimensional groups:

Reynolds Number = $\rho_o \mu_o r_o / \mu_o = R_e$

Prandtl Number = $\mu_o c_{p_o} / \lambda_o = P_r$

Schmidt Number = $\mu_o / D_o \rho_o = S_c$

Collecting all the changes, the nondimensionalized equations

become

$$\frac{\partial}{\partial x}(\rho u) + \frac{1}{r}\frac{\partial}{\partial r}(r\rho v) = 0 \qquad \text{II-(56)}$$

$$\rho u \frac{\partial u}{\partial x} + \rho v \frac{\partial v}{\partial r} = \frac{1}{Re}\frac{1}{r}\frac{\partial}{\partial r}\left(r\mu \frac{\partial u}{\partial r}\right) \qquad \text{II-(57)}$$

$$m u \left[\frac{\partial X_N}{\partial x} + \frac{X_N}{2\bar{X}}\left\{\left(1-2R-\frac{\partial X_A}{\partial X_N}\right)\frac{\partial X_N}{\partial x} - \frac{\partial X_A}{\partial T}\frac{\partial T}{\partial x}\right\}\right]$$

$$+ m v \left[\frac{\partial X_N}{\partial r} + \frac{X_N}{2\bar{X}}\left\{\left(1-2R-\frac{\partial X_A}{\partial X_N}\right)\frac{\partial X_N}{\partial r} - \frac{\partial X_A}{\partial T}\frac{\partial T}{\partial x}\right\}\right]$$

$$= \frac{-1}{Re\,S_c}\frac{1}{r}\frac{\partial}{\partial r}\left[\frac{rm}{\bar{X}}\left\{(R D_{AN} - D_{NA})\frac{\partial X_N}{\partial r} + \left(2\left[D_{NZ} - D_{NA}\right]\right)\frac{\partial X_e}{\partial r}\right\}\right] \qquad \text{II-(58)}$$

$$\rho c_p\left[u\frac{\partial T}{\partial x} + v\frac{\partial T}{\partial r}\right] = \frac{1}{Re\,P_R}\frac{1}{r}\frac{\partial}{\partial r}\left(r\lambda\frac{\partial T}{\partial r}\right) + \frac{P_{rad}}{Re\,P_r} + \frac{1}{Re\,S_c}\frac{\partial T}{\partial r}\frac{1}{T\bar{X}}\cdot$$

$$\cdot\left\{\begin{array}{l}(R D_{AN} - D_{NA})\dfrac{\partial X_N}{\partial r} + 2(D_{NZ} - D_{NA})\dfrac{\partial X_e}{\partial r} \\ + (2R-1)\left[(R D_{AN} - D_{NA})\dfrac{\partial X_N}{\partial r} + 2(D_{NZ} - D_{NA})\dfrac{\partial X_e}{\partial r}\right]\end{array}\right\} + \frac{\bar{X}}{Re\,S_c}\left(1+\frac{I}{T}\right)\cdot$$

$$\cdot\left\{\begin{array}{l}\dfrac{1}{r}\dfrac{\partial}{\partial r}\left[\dfrac{rm}{\bar{X}}\left(\left[R D_{AN} - D_{NA}\right]\dfrac{\partial X_N}{\partial r} + 2(D_{NZ} - D_{NA})\dfrac{\partial X_e}{\partial r}\right)\right] \\ + \left((1-2R)\left[X_N\dfrac{\partial X_A}{\partial X_N} - X_A\right] - \dfrac{\partial X_A}{\partial X_N}\right)\dfrac{\dfrac{\partial}{\partial r}\left[\dfrac{rm}{\bar{X}}\left((R D_{AN} - D_{NA})\dfrac{\partial X_N}{\partial r} + 2(D_{NZ} - D_{NA})\dfrac{\partial X_e}{\partial r}\right)\right.}{\left(1 + X_A - X_N\dfrac{\partial X_A}{\partial X_N}\right)}\end{array}\right. \qquad \text{II-(59)}$$

7. Von Mises Transformation

The Von Mises transformation for steady compressible axially symmetric flow transforms the independent variables from axial and radial coordinates to the axial coordinate and the stream function, ψ , where ψ is defined by:

$$\left(\frac{\partial \psi}{\partial r}\right)_x = \rho u r \qquad \left(\frac{\partial \psi}{\partial x}\right)_r = -\rho v r \qquad \text{II-(60)}$$

$$\psi = 0 \quad \text{at} \quad r = 0$$

The partial derivatives transform into the new coordinate system as follows:

$$\left(\frac{\partial}{\partial x}\right)_r = \left(\frac{\partial}{\partial x}\right)_\psi - \rho v r \left(\frac{\partial}{\partial \psi}\right)_x$$

$$\left(\frac{\partial}{\partial r}\right)_x = \rho u r \left(\frac{\partial}{\partial \psi}\right)_x \qquad \text{II-(71)}$$

(The variables held constant in the partial differentiation are noted only when there is a possibility for confusion). The inverse of the transform is used to obtain the radius from the stream function coordinate system:

$$r = \sqrt{2 \int_0^\psi \frac{d\psi}{\rho u}} \qquad \text{II-(72)}$$

The advantages of using this transform are: (1) the overall continuity equation is identically satisfied, (2) the convective terms are considerably simplified:

$$u \left(\frac{\partial}{\partial x}\right)_r + v \left(\frac{\partial}{\partial r}\right)_x = u \left(\frac{\partial}{\partial x}\right)_\psi \qquad \text{II-(73)}$$

and (3) the velocity component v is eliminated from explicit consideration in all the equations. The disadvantage is that most of the terms on the right side of energy, momentum and helium diffusion equations are made more complex. In particular, the radius r is never completely eliminated from the equations. Hence at every step of a difference solution the solution in the stream function coordinate system must be inverted back into spatial coordinates. However, inspection of the transformed

equations will show that the radius always occurs in the form r^2. If the inversion is made to r^2 instead of r, the necessity of taking numerous square roots is avoided. The saving of computer time by this simple trick is considerable.

8. Centerline Boundary Condition

The centerline boundary condition is that all the physical quantities are bounded and that the first radial derivatives are zero. This condition gives rise to special simplified versions of the general equations which are valid at the centerline. The fluid mechanical equations all contain terms of the form:

$$\frac{1}{r}\frac{\partial}{\partial r}\left[A(r)\, r\, \frac{\partial}{\partial r} B(r) \right] \qquad \text{II-(74)}$$

If the symbolic variables A and B are expanded in a Taylor series in r with the first derivative equal to zero, it is found that in the limit, as r approaches zero, the term becomes:

$$2\, A(r)\, \frac{\partial^2 B(r)}{\partial r^2} \qquad \text{II-(75)}$$

Specific forms of the above are mentioned in the literature for use in "centerline equations". However, the above form is awkward to use. In numerical finite difference solutions the mesh variable is ψ and not r. Surprisingly, this has never been mentioned in the literature available to the authors.

The simpler form can be most easily obtained by expanding

the derivatives in the transformed equations and setting $r = 0$. However, to prove the equality of the two forms, the following analysis is performed:

Transforming the second derivative

$$\frac{\partial^2 B(r)}{\partial r^2} = \rho \mu r \left[\frac{\partial \rho \mu}{\partial \psi} r \frac{\partial B}{\partial \psi} + \rho u r \frac{\partial^2 B}{\partial \psi^2} + \rho u \frac{\partial r}{\partial \psi} \frac{\partial B}{\partial \psi} \right] \quad \text{II-(76)}$$

All the derivatives are bounded at the centerline except $\frac{\partial r}{\partial \psi}$ Therefore the first and second terms will go to zero in the limit as r approaches zero. From

$$\left(\frac{\partial \psi}{\partial r}\right)_x = \rho u r \quad \text{II-(77)}$$

We obtain $$r \left(\frac{dr}{d\psi}\right)_x = \frac{1}{\rho u}$$

So $$\frac{1}{r} \frac{\partial}{\partial r} \left[A(r)\, r \frac{\partial B(r)}{\partial r} \right] = 2 A(r) \rho u \frac{\partial B}{\partial \psi}$$

at the centerline.

The Reynolds number can be eliminated from explicit consideration by the axial coordinate transformation:

$$Z = \frac{x}{Re} \quad \text{II-(78)}$$

Using the Von Mises transformation the momentum equation becomes

$$\frac{\partial u}{\partial Z} = \frac{\partial}{\partial \psi} \left[\mu \rho u r^2 \frac{\partial u}{\partial \psi} \right] \quad \text{II-(79)}$$

At the centerline we have:

$$\frac{\partial u}{\partial Z} = 2 \mu \frac{\partial u}{\partial \psi} \quad \text{II-(80)}$$

The helium continuity equation transforms into:

$$\left[\bar{X} - \frac{X_H}{2}\left(1-2R-\frac{\partial X_A}{\partial X_H}\right)\right]\frac{\partial X_H}{\partial Z} - \frac{X_H}{2}\frac{\partial X_A}{\partial T}\frac{\partial T}{\partial Z}$$

$$= \frac{\bar{X}^2}{S_c}\frac{\partial}{\partial \Psi}\left\{\frac{\rho^2 U r^2}{\bar{X}^2}\left(\left[R D_{HH} - D_{HA}\right]\frac{\partial X_H}{\partial \Psi} + 2\left[D_{HE} - D_{HA}\right]\frac{\partial X_e}{\partial \Psi}\right)\right\} \quad \text{II-(81)}$$

When the ionization is negligible the above equation reduces to:

$$\frac{\partial X_H}{\partial Z} = \frac{\bar{X}^2}{S_c}\frac{\partial}{\partial \Psi}\left\{\frac{\rho^2 U r^2}{\bar{X}^2} D_{HA}\frac{\partial X_H}{\partial \Psi}\right\} \quad \text{II-(82)}$$

The corresponding equations, valid at the centerline, are:

$$\left[\bar{X} - \frac{X_H}{2}\left(1-2R-\frac{\partial X_A}{\partial X_H}\right)\right]\frac{\partial X_H}{\partial Z} - \frac{X_H}{2}\frac{\partial X_A}{\partial T}\frac{\partial T}{\partial Z}$$

$$= \frac{-2\rho}{S_c}\left\{\left[R D_{HH} - D_{HA}\right]\frac{\partial X_H}{\partial \Psi} + 2\left[D_{HE} - D_{HA}\right]\frac{\partial X_e}{\partial \Psi}\right\} \quad \text{II-(83)}$$

$$\frac{\partial X_H}{\partial Z} = \frac{2\rho}{S_c} D_{HA}\frac{\partial X_H}{\partial \Psi}$$

The transformed energy equation is:

$$\left[\frac{1}{T} - \frac{\left(1+I/T\right)\frac{\partial X_A}{\partial T}}{1+X_A+X_H\frac{\partial X_A}{\partial X_H}}\right]\frac{\partial T}{\partial Z} = \frac{\rho}{P_R}\frac{\partial}{\partial \Psi}\left(\rho U r^2 \lambda \frac{\partial T}{\partial \Psi}\right)$$

$$- \frac{P_{rad}}{P_r U} + \frac{\rho U r^2}{S_c T \bar{X}}\left[\begin{array}{l}\left(R D_{AH} - D_{AA}\right)\frac{\partial X_H}{\partial \Psi} + 2\left(D_{HE} - D_{AA}\right)\frac{\partial X_e}{\partial \Psi} \\ -(1-2R)\left[\left(R D_{HH} - D_{HA}\right)\frac{\partial X_H}{\partial \Psi} + 2\left(D_{HE} - D_{AH}\right)\frac{\partial X_e}{\partial \Psi}\right]\end{array}\right]$$

$$+ \left(1+I/T\right)\frac{\bar{X}}{S_c}\frac{\partial}{\partial \Psi}\left[\frac{\rho^2 U r^2}{\bar{X}^2}\left\{\left(R D_{AH} - D_{AA}\right)\frac{\partial X_H}{\partial \Psi} + 2\left(D_{HE} - D_{AH}\right)\frac{\partial X_e}{\partial \Psi}\right\}\right]$$

II-(84)

For negligible ionization this simplifies to:

$$\frac{1}{T}\frac{\partial T}{\partial z} = \frac{\rho}{P_a}\frac{\partial}{\partial \psi}\left(\rho u r^2 \lambda \frac{\partial T}{\partial \psi}\right) + \frac{\rho^2 r^2 \frac{\partial T}{\partial \psi}(1-R)D_{AM}\frac{\partial X_M}{\partial \psi}}{S_c T \bar{X}} \qquad \text{II-(85)}$$

At the centerline we have:

$$\left[\frac{1}{T} - \frac{(1+I/T)\,\partial X_A/\partial X_M}{1+X_A+X_M\,\partial X_A/\partial X_M}\right]\frac{\partial T}{\partial z} = \frac{2\rho\lambda}{P_a}\frac{\partial T}{\partial \psi} - \frac{P_{rad}}{P_r u}$$

$$+ (1+I/T)\frac{2\rho}{S_c \bar{X}}\left[(R D_{AM} - D_{AA})\frac{\partial X_M}{\partial \psi} + 2\left[D_{Ai} - D_{AA}\right]\frac{\partial X_e}{\partial \psi}\right] \qquad \text{II-(86)}$$

$$+ \left\{\frac{(1-2R)\left(X_A \frac{\partial X_A}{\partial X_M} - X_A\right) - \frac{\partial X_A}{\partial X_M}}{1+X_A+X_M\,\partial X_A/\partial X_M}\right\}\left(\left[R D_{MM} - D_{MA}\right]\frac{\partial X_M}{\partial \psi} + 2\left(D_{Mi} - D_{MA}\right)\frac{\partial X_e}{\partial \psi}\right)\Bigg]$$

which becomes, at low temperature,

$$\frac{1}{T}\frac{\partial T}{\partial z} = \frac{2\rho\lambda}{P_a}\frac{\partial T}{\partial \psi} \qquad \text{II-(87)}$$

The system of three simultaneous parabolic partial differential equations is solved by finite difference techniques. The type selected is the simple two-level explicit forward difference scheme. A full discussion of the finite difference technique and the reason for the selection of the method used is given in Appendix B of Reference 11.

B. EXPERIMENTAL TECHNIQUES

The general experimental approach and the operation of equipment was described in detail in Reference 1. To recall briefly, a commercial plasma gun generates a one-centimeter-diameter jet of partially-ionized argon which exhausts into a reservoir tank of helium. A calorimetric probe is used to survey the mixing region for composition, velocity, and enthalpy, and schlieren photographs are used to verify that the generator is delivering a jet in the laminar mode.

Initial experiments were made with a Model F-80 plasma torch manufactured by Thermal Dynamics, Inc. This device was generally suitable for measurements close to the nozzle, but at a few inches downstream the jet was not sufficiently stable to permit collection of reproducible data. For this reason a new plasma generator made by Creare, Inc., was purchased. The Creare plasma generator, shown in Figure 3 and installed in Figure 4, incorporates the features of complete micrometer adjustment of the cathode position and a straight-line nozzle consisting of insulated sections, permitting selection of anode location. The best laminar jet was obtained when the last segment was selected as the anode, using ten 1/4-inch-thick segments. The generator was operated at an argon flow rate of 0.3 grams per second and at a power of 14 kw. Peak values for temperature and velocity at the nozzle exit plane were 20,000°R and 550 feet per second, respectively, The initial peak ionization fraction was 0.07.

As described in Reference 1,a schlieren system was built to establish the general nature of the flow as affected by the operating conditions of the plasma generator and the design of the anode-nozzle. The system was found adequate to distinguish density gradients of the argon arcjet flowing into nitrogen, but was barely adequate for helium, since in mixtures of cool helium and hot argon the density gradients were so small as to be at the limits of the system's resolution. Figure 2 is a schlieren photograph showing a typical laminar

argon jet in nitrogen and its transition to turbulence. Schlieren photographs of the arcjet in helium were presented in References 1 and 11.

The probe measurements were conducted, as in previous work, by surveying radial profiles at axial distances from the exit plane of 1/32,5/16,1/2,1,2,3, and 4 inches. Profiles to 4 inches downstream were also taken using the Thermal Dynamics generator, but since the Creare generator data were generally more consistent and reliable, particularly at distances greater than two inches from the nozzle exit plane, only these data are reported here. Thermal Dynamics data are reported in Reference 11, and support the conclusions based on the Creare data. Measurements of centerline values of temperature, velocity, and composition were made with the Creare generator to a downstream axial location of six inches.

C. DISCUSSION OF RESULTS

Experimental and theoretical results are compared in Figures 5 through 15. Figures 5,6,7, and 8 plot centerline values of temperature, enthalpy, velocity, and composition, respectively, and also include results of similar jet mixing studies performed in a 3-inch round duct. The duct mixing studies at the coaxial helium velocity flow of 0.27 feet per second closely correspond to the free jet case, because at this flow velocity turbulence effects of the coaxial gas did not disturb the laminar quality of the jet, but the ambient helium concentration was sufficient to provide close resemblance to the free-jet case. Similarities between the free jet and the ducted jet for other coaxial velocities do not exit because at high coaxial (helium)

velocities the jet became turbulent, whereas at zero coaxial velocity in the duct the helium environment was swept out by the jet. The duct mixing experiments, performed for NASA, are described in detail in Reference 9 . A significant result of all these studies is illustrated by Figure 6. This figure shows that in all cases of duct mixing, as well as for the free jet, the centerline enthalpy decay is the same. This is an important verification of the mechanism of mixing as proposed by the theoretical analysis, and will be discussed in detail later.

The experimental and theoretical profiles of temperature, velocity and composition are shown in Figures 9 through 15 for axial locations starting at 1/32-inch downstream from the nozzle exit and proceeding at intermediate intervals to five inches downstream. For purposes of the theoretical computations the 1/32 inch experimental profiles were used as the basis for the initial profiles required by the computation technique. The agreement between theory and experiment is satisfactory, the lack of consistency in the concentration data resulting from the unavoidable buildup of argon in the ambient helium atmosphere during the performance of the tests. A composition curve which has been normalized to the tank reference value is also shown on the composition plots, and agreement between this curve and the data is good.

Both the theoretical study and interpretation of the results support the hypothesis that the basic process of mixing

is an inflow of ambient helium into the argon arcjet rather than loss of jet energy by radiation or by dispersion of the argon. This behavior is probably due to the large specific heat of the helium and the strong dependence of the diffusion coefficients on temperature, which tend to dominate any effects due to changes in the amount of radiation or the energy of ionization.

As mentioned previously, experimental verification of this mechanism is best evidenced by reference to Figure 6. Even though the various jet configurations studied differed widely in terms of centerline values of temperature, velocity, and concentration (Figure 5,7, and 8), the centerline enthalpy decays of all cases coincide almost identically, Such a result indicates that radiation and ionization effects are indeed negligible, since reference to Figure 5 shows that the jet temperatures differ by many thousands of degrees at only short distances downstream of the nozzle exit plane. For example, at one inch from the nozzle, the temperatures of the jets which were still considered laminar were about 11,000°R, while that of the turbulent jet, in which mixing was substantially complete, was only 1,000°R; yet the enthalpies at the centerline were the same. Clearly, if radiation and ion recombination effects were important mechanisms for jet power loss, the higher temperature jets should show lower enthalpies. On the other hand, if there were substantial dispersion of the arcjet the centerline enthalpy of the well-mixed case should be substantially

less.

It is, however, conceivable that domination of the mixing process by the helium inflow may have resulted from the very low helium-to-argon velocity ratio; e.g., from the comparatively long "stay time" of the helium in the neighborhood of the jet. This possibility is being investigated under a current NASA research program, part of which will consist of tests with high ratios of coaxial to core-gas velocity.

III. THEORY OF AN ELECTROSTATIC PROBE IN A DENSE PLASMA

A. INTRODUCTION

This section discusses a new technique for the diagnostics of a dense plasma (mean free path much smaller than the probe diameter). There has been a great deal of work, over a period of about 50 years, devoted to measurements within electrical discharges. However, most of the theoretical work and virtually all of the experimental efforts have been directed at ionized gases of very low density.

In order to measure the local properties of a dense plasma, entirely new methods must be used. For reasons which are discussed below, spectroscopic and microwave techniques must be rejected. The use of a classical Langmuir probe is impossible due to the thermal limitations of all known conducting materials. It was therefore considered worthwhile to investigate the use of a cooled electrostatic probe with a view toward obtaining accurate, repeatable measurements capable of point-by-

point resolution and disturbing the free-stream conditions as little as possible. The theory of such a device is derived in this section.

The fundamental physical problem we wish to study is the degree of nonequilibrium present in an argon plasma at a pressure of one atmosphere. By nonequilibrium we mean the difference between the electron temperature and the heavy particle temperature (32,33,34). Due to the effective energy transfer by elastic collisions for particles of nearly equal mass, the electrons will be in a Maxwellian distribution appropriate to a temperature T_e, and the argon atoms and argon ions in a Maxwellian distribution appropriate to the heavy particle temperature T_H(35). We then desire an accurate determination of (T_e-T_H) over the region occupied by the plasma. In a sense, the purpose of this section is to determine if this measurement can be performed with a cooled electrostatic probe.

The local heavy particle temperature (the usual temperature associated with a non-ionized gas) has been measured accurately using the calorimetric probe discussed in previous reports (1, 2, 11). Therefore, since the heavy particle temperature can be established locally, the essential problem becomes that of a local determination of the electron temperature. Alternate methods to the cooled electrostatic probe have been considered, but have been rejected after careful review. Spectroscopic techniques such as Stark or Doppler broadening are not suitable

for a number of reasons. The first difficulty lies in the fact that in argon there are higher order Stark effects (36). Further, the Stark effect furnishes information as to the value of the ionization density, and the Doppler effect gives information on the ion temperature. Thus the electron temperature can be determined only for the case of equilibrium, which masks the basic question concerning the extent of non-equilibrium. Spectroscopic methods are also quite delicate and are subject to the usual line-of-sight problem which makes local measurements very difficult in a plasma with extremely high gradients and possible asymmetries.

Microwave techniques, while quite useful at very low particle densities, become useless in the range of greatest interest ($n_e \approx 10^{15}$ electrons/cm^3). This is due to the state-of-the-art limitations on the available frequencies of the microwave equipment. Microwave techniques are also subject to the same depth-of-field limitations which occur in spectroscopic measurements.

Therefore, the most appropriate technique appears to be the electrostatic probe modified to meet the requirements of a dense plasma. The literature concerning both the theory and application of this device [(see References 36-43)] is quite extensive for the case of very low pressure. However, for higher pressures there are virtually no experimental results, and very little in the way of theory. Some of the more recent work (see References 44-50) attempt advances in this direction,

but none of these is truly appropriate for the case of a one-atmosphere plasma.

The reason for the meager amount of data in dense plasmas is the simple fact that probes melt. The classical Langmuir probe is essentially just a thin wire conductor immersed in a plasma. At particle densities of 10^8 - 10^{12} particles/cm^3 the energy flux striking the probe is very low, despite the high "temperatures" of the plasma. The probe is able to withstand this energy flux due to its thermal heat capacity, and in some cases, short durations of exposure. However, at particle densities of 10^{15} - 10^{18} at approximately the same temperatures, the heat flux to a bare wire is so enormous as to melt the wire. The logical step, in light of the successes attained with the calorimetric probe under these conditions, appeared to be a water-cooled electrostatic probe. The word "electrostatic" is used here in place of "Langmuir" because the device to be used is sufficiently different from the classical Langmuir probe as to warrant a separate designation. The two instruments are similar in many respects, but there are certain fundamental points in which great differences are observed.

In a dense plasma the particle densities are sufficiently high to produce a collision-dominated regime; i.e., continuum fluid mechanics. The flow conditions near the cooled probe are satisfied by the usual momentum and thermal boundary layer models. In order to satisfy the "no-slip" condition, the

velocity of the gas at the probe surface must vanish, and the temperature of the neutral gas atoms must be very nearly equal to the temperature of the probe surface itself. Further, due to the great number of collisions and the nearly-equal masses of the atoms and the ions, the ions will also follow the usual boundary layer temperature profile. The electrons, on the other hand, being $1/72{,}000^{th}$ the mass of the atoms, will in general be less affected by the presence of the cool probe.

This coupling between the fluid mechanics of the boundary layer region and the electrostatics of the probe and plasma represents the major theoretical problem to be solved. Each of these problems is exceedingly difficult in its own right, and the combined problem becomes virtually intractable in terms of a general solution. Fortunately, we may separate certain aspects of the problem, and with the help of some simplifying assumptions, we can obtain an approximate theory which appears to provide a reasonably accurate description of the physical phenomena occurring in the neighborhood of a cooled probe.

B. THEORY OF THE CLASSICAL LANGMUIR PROBE

In order to gain a better appreciation for the problem, the following typical properties, speeds, and characteristic lengths are suggested:

PROPERTIES	SPEEDS	LENGTHS
T_∞ = 12,000°K	$\bar{c}_e = 7 \times 10^7$ cm/sec	L probe = 10^{-1}cm
T_{wall} = 300°K	$\bar{c}_i = 2.5 \times 10^5$ cm/sec	$\delta_{thermal} = 1.0 \times 10^{-2}$cm
ρ = 1 atm	$v_\infty = 3 \times 10^4$ cm/sec	$\lambda_{elec\text{-}atom} = 1.43 \times 10^{-3}$cm
$n_{A_\infty} = 6 \times 10^{17}$cm^{-3}		$\lambda_{elec\text{-}ion} = 1.5 \times 10^{-4}$cm
$n_{A_{wall}} = 2.7 \times 10^{19}$cm^{-3}		$h_{Debye} = 2.87 \times 10^{-6}$cm
$n_{i_\infty} = 2.1 \times 10^{16}$cm^{-3}		$\bar{P}_o = 5.5 \times 10^{-8}$cm
$n_{i_{wall}} = 1.3 \times 10^{17}$cm^{-3}		
$\alpha_\infty = 0.033$		

(cross-section data for the calculation of the mean free paths are taken from references 51, 52, and 53.)

Now, according to the basic concept of Langmuir et. al. (37-40), the electrostatic problem may be divided into two regions. Far from the probe any potentials applied to the probe are screened by the presence of a "sheath" surrounding the probe. This "electrostatic boundary layer" is a region composed primarily of charges of one sign. If the probe is made positive with respect to the surrounding plasma, an electron sheath will form near the probe and the ions will be repelled. If the probe is made negative, an ion sheath will form and will exclude all but the most energetic electrons.

The separation into a sheath and undisturbed plasma has many important ramifications. Since, by definition, the electric fields do not penetrate into the undisturbed plasma, and since total charge must be conserved, then we obtain

in the undisturbed region:

$$\rho_{TOT} \equiv \rho_+ + \rho_- = 0 \qquad \text{III-(1)}$$

where ρ is charge density.

For a singly ionized gas $\rho_+ = \varepsilon_i m_i$ and $\rho_- = \varepsilon_e m_e$ Since the electron charge is equal to - e ion,

$$m_e = m_i \qquad \text{III-(2)}$$

Further, according to Langmuir's theory the entire potential drop between the biased probe and the neutral plasma occurs within the sheath. On the basis of this separation of the sheath region and neutral plasma region one may now consider the nature of the variation of the current drawn by the probe as its potential is varied from $-\infty$ to ∞.

The total current I to the probe is given by

$$I = I_e + I_i \qquad \text{III-(3)}$$

We shall adopt the convention that positive charge moving away from the probe is positive current. Thus negative charge (electrons) moving towards the probe is positive current and positive charge (ions) moving towards the probe is negative current.

Now, for a species j which is in a self-Maxwellian distribution the following relations apply

$$I_j = \iint j_j \, dS \qquad \text{III-(4)}$$

where j_j is the current density (amperes/cm^2). In the presence of purely thermal motions (i.e., in a region where both the potential and the electrostatic fields are zero) it

is well-known that the random current density is

$$(j_R)_j = \frac{1}{4} \varepsilon_j n_j \bar{c}_j \qquad \text{III-(5)}$$

Finally, if these particles exist in a region where the potential is V volts relative to the neutral plasma, then the population in this region is given by the well-known Boltzmann distribution

$$n_j = n_{j_0} e^{\varepsilon_j V / k T_j} \qquad \text{III-(6)}$$

where T_j is defined by

$$\frac{1}{2} m_j \overline{c_j^2} = \frac{3}{2} k T_j$$

From Reference (54) we find

$$\bar{c}_j = \sqrt{\frac{8 k T_j}{\pi m_j}} \qquad \text{III-(7)}$$

Therefore, substituting Eqs III-(6) and III-(7) into Eq III-(5)

$$j_i = \varepsilon_j n_{j_0} \sqrt{\frac{k T_j}{2\pi m_j}} e^{\varepsilon_j V / k T_j} \qquad \text{III-(8)}$$

Setting j = "electron" and "ion" respectively, and employing Eq III-(2), we find, at a point where $V = 0$,

$$(j_R)_e = (j_R)_i \sqrt{\frac{m_i}{m_e} \frac{T_e}{T_i}} \qquad \text{III-(9)}$$

where the R-subscript appears whenever V = o, and therefore applies to neutral plasma conditions. Since the energy of the arc initially goes into the electrons, it is apparent that the electron temperature must be greater than, or at least equal to, the ion temperature. Thus the random electron current must be $\geq (m_i/m_e)^{1/2}$ times the random ion current. For argon $(m_i/m_e)^{1/2}$ = 271. Therefore, assuming ideal conditions such as constant probe area, uniform current density over the surface of the probe, no "end effects", and separate Maxwellian distributions for ions and electrons, we may construct the curves of Figure 16.

These curves are not to scale, since for argon $(I_R)_e$ should be at least 271 times as great as $(I_R)_i$. Note that the ion current to the probe is negative and the electron current to the probe is positive, according to our convention. The curves show an exponential decay in the regions of repelling potential (exponentially fewer particles have sufficiently high energy to surmount the potential barrier of the sheath and "drift" to the probe). The curves show a flat portion in the attracting region. This is because all the particles in the immediate vicinity are being captured by the probe, which clearly cannot capture any more without making new ones. This indeed can happen. At positive potentials greater than the ionization potential (15.76 volts for argon) or, in the case of multiple-step ionization, the excitation potential (11.4 volts for argon), the electrons can gain so much energy in "falling" thru this potential as

to cause additional ionization. This now releases an extra electron and ion pair. The electron is (generally) captured by the positive field while the ion is repelled. This causes an increase in the current collected by the probe as shown by the dashed line in Figure 16-B. However, this occurs at potentials beyond the normal operating range, and is not of great interest.

From Eq III-(30) the sum of these curves should give the total current drawn by the probe as a function of voltage. This is known as a current-voltage characteristic. A typical characteristic for an ideal Langmuir probe is shown in Figure 17. From Figure 17 it is apparent that there must exist some unique value of potential Φ_F such that the total current drawn by the probe is zero. Since the area of the probe is constant, this will occur when

$$-j_i(\Phi_F) = j_e(\Phi_F) \qquad \text{III-(10)}$$

$$j_i = -\varepsilon_i \cdot n_{i_0} \bar{c}_i / 4$$

$$j_e = \varepsilon_e n_{e_0} \frac{\bar{c}_e}{4} e^{-|\varepsilon_e \Phi_F| / k T_e}$$

Using the neutrality condition, Eq III-(2)

$$\left[\frac{8kT_i}{m_i}\right]^{1/2} = \left[\frac{8kT_e}{m_e}\right]^{1/2} e^{-|\varepsilon_e \Phi_F| / k T_e}$$

or

$$\Phi_f = - \frac{k T_e}{\varepsilon_e} \ln \left[\frac{m_i}{m_e} \frac{T_e}{T_i} \right]^{1/2} \qquad \text{III-(11)}$$

For an argon plasma at one atmosphere and about 12,000°K, $\Phi_f \approx$ - 6 volts.

Furthermore, from Eq III-(8) (for electrons) one can easily see that

$$\ln I_e = \ln \left[A_p \varepsilon_e N_{e_0} \sqrt{\frac{k T_e}{2 \pi m_e}} \right] + \varepsilon_e V / k T_e \qquad \text{III-(12)}$$

or

$$\frac{d \ln I_e}{dV} = \varepsilon_e / k T_e \qquad \text{III-(13)}$$

Therefore, the slope of the semi-logarithmic plot of current versus voltage allows one to determine the electron temperature of a swarm of electrons in a Maxwellian distribution.

Knowing the electron temperature, one can then deduce the average electron speed and, having measured the probe current and probe area, the electron density can be calculated from Eq III-(5), provided one uses the value for I_{Re} at zero potential. From the neutrality condition this immediately gives n_i. In principle, the Langmuir probe can also be used to determine the ion temperature, but this measurement has not been very successful (32,36,42,48).

C. THE COOLED ELECTROSTATIC PROBE

We have just shown that the classical Langmuir probe permits the determination of the electron temperature when the pressure is sufficiently low that the mean free path is much greater than the dimensions of the probe. This implies that there is little or no boundary layer. However, in the case of interest the flow is very definitely continuum, the mean free path is much smaller than the probe, and a thermal boundary layer exists. These differences are summarized below, where L = typical probe dimension:

	Pressure	Mean Free Path	Boundary Layer	Collisions
Langmuir Probe Conditions	10^{-5}-10^{-6} atm	$\lambda > L$	No	Rare
Cooled Probe Conditions	1 atm	$\lambda << L$	Yes	Very Common

The basic question then becomes, "How does the presence of a boundary layer affect the interpretation of the results obtained with an electrostatic probe?" In order to answer this question, we must examine the effect of collisions upon the history of a test particle starting from the neutral plasma and eventually arriving at the probe.

We first separate the problem into four regions as shown in Figure 18.

It has been recognized for some time (see References 41,

42, 44, 45, 48 and 49) that one of the major defects of the Langmuir theory is the fact that potential differences are not fully confined to the sheath; i.e., the effects of the probe are actually felt at greater distances. This leads to Bohm's concept of a transition region, which is defined in such a manner (see Reference 41) that the fields beyond d are smaller than the variations of thermal energy over an electron-ion collisional mean free path. That is, if x is the distance from the probe, at $x = d$

$$\mathcal{E} \leq V_e/\lambda \qquad \text{III-(14)}$$

where $V_e \equiv k T_e/\varepsilon_e$

Confining ourselves to the transition region, where the currents are dominated by local electric fields rather than by random thermal motions, we may write (subscript zero denotes regions in which $V = o$)

Mobility Expression $\qquad \nu(x) = b \frac{dV(x)}{dx} \qquad$ III-(15)

Current Continuity $\qquad M_o \varepsilon N_o = M(x) \varepsilon N(x) \qquad$ III-(16)

Boltzmann Distribution $\qquad M(x) = M_o e^{-V(x)/V_e} \qquad$ III-(17)

Combining III-(16) and III-(17) with III-(15)

$$N(x) = N_o e^{+V(x)/V_e} = b \frac{dV(x)}{dx} \qquad \text{III-(18)}$$

or

$$\int_0^x \frac{N_0}{b}\, dx = \int_0^{V(x)} e^{-V/V_e}\, dV$$

Assuming b = constant (see Reference 54) we find, after some algebra

$$1 - e^{-V(x)/V_e} = \frac{N_0}{b}\,\frac{x}{V_e} \qquad \text{III-(19)}$$

Employing Bohm's Sheath Criterion (Eq III-14)

$$dV(x)/dx = V_e/\lambda$$

at x = d, we substitute into Eq III-(18) and find

$$\left.\frac{dV(x)}{dx}\right|_{x=d} = \frac{N_0}{b}\, e^{+V(d)/V_e} \qquad \text{III-(20)}$$

and, at x = d

$$\frac{dV}{dx} = \frac{V_e}{\lambda} = \frac{N_0}{b}\, e^{+V(d)/V_e}$$

or

$$V(d) = V_e \ln\left\{\frac{b V_e}{N_0 \lambda}\right\} \qquad \text{III-(21)}$$

Solving Eq III-(19) for V(d) we obtain

$$V(d) = -V_e \ln\left\{1 - \frac{N_0 d}{b V_e}\right\} \qquad \text{III-(22)}$$

Solving Equations (21) and (22) simultaneously, we find, after some algebra

$$\frac{d}{\lambda} = \frac{b V_e}{N_0 \lambda} - 1 \qquad \text{III-(23)}$$

Using appropriate values one can show that (41)

$$0 < d < 2\lambda$$

so that the thickness of the transition region is of the order of the mean free path for electron-ion collisions.

We now note the reason for the seemingly arbitrary division into four regions. Using the typical values given earlier, we note that:

Boundary Layer Thickness $\approx$ 100 x Transition Region Thickness

Transition Region Thickness $\approx$ 20 x Sheath Thickness

It is of interest to point out that the space-charge-limited equation (Ref. 37)

$$j = \frac{1}{9\pi}\left(\frac{2\epsilon}{m}\right)^{1/2}\frac{V^{3/2}}{x^2}\left(1 + 2.66\,\frac{kT}{\epsilon V}\right) \qquad \text{III-(24)}$$

gives a value of $x = 5.24 \times 10^{-5}$cm for an argon plasma at 1 atm and 12,000°K with V = 30 volts.

The sheath itself is of the order of the Debye length based upon free-stream conditions (49). The Debye length is given by the expression (52,53)

$$h = \sqrt{\frac{kT}{4\pi n_e \epsilon^2}} \qquad \text{III-(25)}$$

and under these conditions is 2.87×10^{-6}cm. Therefore x/h = 18, and taking x = d, we find $d \approx \lambda/3$. These results are in excellent agreement with the work of References 45 and 61.

The essential philosphy of the division into 4 regions is therefore as follows:

A. The free-stream plasma is beyond the region of probe disturbances (electrostatic or fluid mechanical). This is the region we really want to learn something about.

B. The boundary layer accounts for the entire fluid mechanical transition, and yet there are no electrostatic effects, since these do not extend beyond the transition region.

C. The transition region is a region in which the electrostatic field becomes important in "drawing in" particles of the proper charge. Since the transition region is smaller than an electron-ion mean free path, there will be few or no collision during this region.

D. The sheath is a region of very large electric fields which act to repel or attract particles of the appropriate sign. Once an attracted particle has reached the sheath it will always reach the probe.

We now consider four cases related to the collison history of an electron originating in the free stream plasma and proceeding towards a positively charged probe under the following assumptions:

(1) The heavy particle temperature T(y) has the usual boundary layer shape, dropping to T_{wall} at y = o and equal to T_∞ at y = δ .

(2) The electron temperature in the free stream plasma is of the same order as the heavy particle temperature in the free stream plasma. This assumption is <u>not</u> essential but is convenient in establishing a simple basis for the model.

(3) $\delta \gg h$

(4) Electrons within the sheath are captured by the applied positive potential.

These assumptions are illustrated by Figure 19.

Case I. <u>No Recombination</u>

This corresponds to the situation in which the residence time of the electron in the vicinity of positive ions is shorter than the characteristic time for recombination

(The various mechanisms of recombination will be treated in Case II).

Further:

(a) The neutral atoms form a boundary layer since the probe is cold.

(b) The ions are in equilibrium with the neutral atoms as a result of the large number of highly effective neutral-ion collisions.

(c) The electrons lose energy to the heavy particles by electron-heavy particle elastic collisions but do not suffer recombination.

For reasonable degrees of ionization, electron-ion collisions are much more probable than electron-neutral collisions due to the large coulombic cross-sections (32,55). Although the values may not be precise, at the conditions of interest Massey and Burhop (51) give the following values for these cross sections:

$$\sigma_{e\text{-}A} = 10^{-16} \text{ cm}^2$$

$$\sigma_{e\text{-}i} = 3 \times 10^{-13} \text{ cm}^2$$

Since the masses of the ions and neutrals are virtually the same, therefore, energy transfer by elastic electron-ion collisions will be dominant relative to energy transfer by elastic electron-neutral collisions whenever the ionized fraction exceeds 0.001. This will be true for temperatures greater than about 8,000°K (55, 56).

The fraction of initial electron energy lost by the electron to the ion in a single electron-ion collison is given by the following expression(54):

$$\left(\frac{\overline{\Delta E}}{E_o}\right) = \overline{F(\chi)} \cdot \frac{4\, m_e m_i}{(m_e + m_i)^2} \qquad \text{III-(26)}$$

where $4\frac{m_e m_i}{(m_e+m_i)^2}$ = fraction of energy lost in a head-on collision between the electron and ion.

χ = deflection angle

$\overline{F(\chi)}$ = average steric factor, taking into account the average overall deflection angles., = 1/2.

Thus

$$\left(\frac{\overline{\Delta E}}{E_o}\right) \approx 2\,\frac{m_e}{m_i} \qquad \text{III-(27)}$$

where we have neglected the mass of an electron relative to the mass of an ion wherever the two are added.

For argon $\frac{m_i}{m_e} = 39.94 \times 1832$

Thus

$$\left(\frac{\overline{\Delta E}}{E_o}\right) = \frac{1}{36,640}$$

Now, in the first collision

$$\left(\frac{\overline{\Delta E}}{E_o}\right)_{coll.} \equiv \frac{E_o - E_1}{E_o} = 1 - \frac{E_1}{E_o} = \frac{1}{36,640}$$

or

$$E_1 = E_o\left\{1 - \frac{1}{36,640}\right\} \equiv \alpha E_o$$

For the second collision

$$\left(\frac{\overline{\Delta E}}{E_0}\right)_{coll.} \equiv \frac{E_1 - E_2}{E_1} = 1 - \frac{E_2}{E_1} = \frac{1}{36,640}$$

or

$$E_2 = E_1 \left\{1 - \frac{1}{36,640}\right\} = \alpha E_1 = \alpha^2 E_0$$

Similarly for the third collision $E_3 = \alpha^3 E_0$

and therefore for the N^{th} collision

$$E_N = \alpha^N E_0 \qquad \text{III-(29)}$$

where $\alpha \equiv \left\{1 - \frac{1}{36,640}\right\}$ and E_0 = initial electron energy.

Expanding, using the binomial theorem and neglecting terms of order $[N/36,640]^2$ and higher with respect to unity, we obtain

$$E_N = E_0 \left\{1 - \frac{N}{36,640}\right\} \qquad \text{III-(30)}$$

We must now calculate the number of electron-ion collisions an electron experiences in travelling from the edge of the boundary layer to the probe surface.

Number of Electron-Ion Collisions

Since the mean free path for electron-ion collisions is a function of temperature and ion density, which are themselves functions of position in the boundary layer, this implies a variation of mean free path with position.

We can evaluate the mean free path in the free-stream plasma in terms of T_∞ , $n_{e\infty}$ and $n_{A\infty}$. These quantities can be calculated from the Saha Equation, provided the degree of nonequilibrium in the free plasma is small. Once these quantities have been calculated, we can begin an iteration scheme to determine the number of electron-heavy particle collisions suffered by an electron in traversing the boundary layer.

To a first approximation the number of collisions is given by

$$(N)_1 = \sqrt{6}\ \delta/\lambda_\infty$$

The factor of $\sqrt{6}$ accounts for the increase in effective path length due to the three-dimensional movement of the electron (36). The quantity $\frac{\delta}{\lambda_\infty}$ is the thickness of the region of interest in multiples of the free-stream mean free path. This is clearly an approximate result, since it does not take into account the variation of the mean free path through the boundary layer. Using actual Ramsauer cross-section data, we obtain the table on the next page.

Inserting these values of $(N)_1$ into equation III-(30) it is immediately apparent that the electrons suffer so few collisions in traversing the boundary layer that they lose very little of their energy. For the typical case, T_∞ = 12,000°K $(N)_1$ = 163 and E_f = 0.996 E_o. It seems clear that even allowing for variability of λ throughout the boundary layer, the electron

ELECTRON MEAN FREE PATH

T_∞ (°K)	α_∞	n_{e_∞} (cm^{-3})	n_{A_∞} (cm^{-3})	λ_∞ (cm)	(N),
13,500	.100	5×10^{16}	4.5×10^{17}	6.7×10^{-5}	365
12,000	.033	2.1×10^{16}	6.0×10^{17}	1.5×10^{-4}	163
10,500	.010	7.1×10^{15}	7.1×10^{17}	4.6×10^{-4}	53
8,500	.001	8.0×10^{14}	8.0×10^{17}	1.0×10^{-4}	25
7,200	10^{-4}	1.0×10^{14}	1.0×10^{18}	1.0×10^{-3}	25
6,100	10^{-5}	1.3×10^{13}	1.3×10^{18}	1.0×10^{-3}	25
5,200	10^{-6}	1.5×10^{12}	1.5×10^{18}	1.0×10^{-3}	25
1,000	10^{-13}	10^{6}	7.2×10^{18}	7.3×10^{-4}	33
300	10^{-13}	10^{6}	2.7×10^{19}	1.8×10^{-4}	130

where δ = 0.010 cm (calculated from the stagnation point boundary layer theory of Ref. 58)

p = 1 atm

NOTE

Actual Ramsauer cross-section data for argon (11) were used. Values for $\sigma_{e\text{-}A}$ and $\sigma_{e\text{-}i}$ are based on the electron energy. Due to the Ramsauer effect, the mean free path for atom-atom collisions is about 1/10th the values given above, so there are about 250 atom-atom collisions in a boundary layer with T_∞ = 7,000°K.

temperature will be nearly constant in this region.

Now, the ionization and recombination rates in a partially ionized gas depend essentially on the relative velocity of the colliding electron-ion pair. This relative velocity is almost entirely the velocity of the electron (within about 1 part in $[m_i/m_e]^{1/2}$) and is almost independent of the motions of the ions. The electron velocity in the boundary layer depends solely upon the electron temperature in the boundary layer, since this region is outside the domain of electric field effects. Since the first iteration yields $T_e \approx$ const $\approx T_{e_\infty}$ through the boundary layer, we may use the Saha equation, but with the electron temperature T_e. This implies, as stated above, that the ionization or recombination process is in equilibrium about the electron temperature even though the atoms and ions may be much "cooler" throughout the boundary layer.

The Saha Equation gives

$$\frac{m_e M_i}{M_o} = K(T_e) \qquad \text{III-(31)}$$

where $M_o = M_A + M_i$

The neutrality condition $m_e = m_i$ applies throughout the boundary layer, except for the very thin transition region. Therefore

$$m_e^2 = (M_A + M_e)\, K(T_e) \qquad \text{III-(32)}$$

Since the entire plasma is at constant pressure in the subsonic free-jet flow, Dalton's law provides

$$p = p_e + p_i + p_A \qquad \text{III-(33)}$$

where the perfect gas law takes the form

$$p_e = n_e k T_e$$
$$p_i = n_i k T_i \qquad \text{III-(34)}$$
$$p_A = n_A k T_A$$

Applying the neutrality condition $n_e = n_i$, the heavy-particle equilibrium requirement $T_i = T_A$, and the result of the first iteration, $T_e = T_{e_\infty} = \text{const}$, we find

$$n_e (T_{e_\infty} + T_A) + n_A T_A = \text{const} \qquad \text{III-(35)}$$

Equations III-(33) and III-(35) represent two equations in the two unknowns n_e and n_A in terms of the independent variable T_A. If we assume a boundary layer heavy-particle temperature distribution (e.g., the function $T_A = T_A(y)$ may take a Blasius-like form) then we expect solutions of the form $n_e(y)$ and $n_A(y)$. The exact solutions for an arbitrary degree of ionization are given (after considerable algebraic manipulation) by

$$n_A(y) = \tilde{n}(y) - \tilde{\tilde{n}}(y) \qquad \text{III-(36)}$$

and

$$n_e(y) = \frac{K_0}{2}\left[1 + \sqrt{1 + \frac{4 n_A(y)}{K_0}}\right] \qquad \text{III-(37)}$$

where

$$\tilde{m}(y) \equiv p_0 / k T_A(y)$$

$$\tilde{n}(y) \equiv n(y) \left[\sqrt{1 + \frac{2\tilde{m}}{n}(1 + T_A/T_\infty)} - 1 \right]$$

$$n(y) \equiv \frac{T_\infty}{T_A(y)} \left[1 + \frac{T_\infty}{T_A(y)} \right]^{\frac{K_0}{2}}$$

Within an error of the order of the degree of ionization, we may, for small ionization, simplify these expressions to the following:

$$m_A = \frac{p_0}{k T_A} \qquad \text{III-(38)}$$

$$m_e = \sqrt{K_0}\ m_A^{1/2} \qquad \text{III-(39)}$$

We may now perform a second iteration to include the variability of the mean free path.

The number of collisions suffered by an electron in travelling a "crow-flight" distance dy is

$$dN = \frac{\sqrt{6}}{\lambda}\, dy \qquad \text{III-(40)}$$

where

$$\lambda = \frac{1}{m_e \sigma_{e-i} + m_A \sigma_{e-A}} \qquad \text{III-(41)}$$

for collisions between electrons and either atoms or ions. We now write Equations III-(38), (39) in the form

$$M_A = M_{A_\infty} \left(\frac{T_\infty}{T_A} \right) \qquad \text{III-(42)}$$

$$M_e = M_{e_\infty} \left(\frac{T_\infty}{T_A} \right)^{1/2} \qquad \text{III-(43)}$$

Thus $$(N)_2 = \sqrt{6} \int_0^\delta \frac{dy}{\lambda(y)} = \sqrt{6} \int_{T_{WALL}}^{T_\infty} \frac{1}{\lambda} \left(\frac{dy}{dT_A} \right) dT_A \qquad \text{III-(44)}$$

where $(\ )_2$ indicates second order iteration and the quantity $\left(\frac{dy}{dT_A} \right)$ depends solely upon our choice of boundary layer heavy-particle temperature variation.

The cross-section $\sigma_{e-i} = \pi^3 e^4 \ell n \Lambda / 8 (kT_e)^2$ (see Ref. 52), where $\Lambda \equiv h/\bar{P}_0$ and $\bar{P}_0 \equiv e^2/3kT_e$, is taken constant through the boundary layer, since $T_e \approx$ const and $\ell n \Lambda$ varies very little.

Similarly $\sigma_{e-A} = \sigma_{e-A}(T_e)$ is also taken constant due to the approximate constancy of the electron temperature as given by the first order iteration. Nonetheless it is important to note that while this cross-section is taken to be constant through the boundary layer, the effect of different values for T_{e_∞} is accounted for by using actual Ramsauer data.

In order to evaluate the effect of the variability of the mean free path and the sensitivity to the actual shape of the assumed atom temperature through the boundary layer, we proceed as follows.

Define

$$\theta \equiv \frac{T_A - T_{A\,wall}}{T_{A\infty} - T_{A\,wall}} \qquad \text{III-(45)}$$

and

$$y = \delta\, \theta^s \qquad \text{III-(46)}$$

The boundary conditions are as follows:

when $y = 0$, $\theta = 0$ and $T_A = T_{A\,wall} = T_w$

when $y = \delta$, $\theta = 1$ and $T_A = T_{A\infty}$

Further,

$$\frac{dy}{dT_A} = \frac{s\,\delta}{(T_\infty - T_w)^s}\,(T_A - T_w)^{s-1}$$

If we also define

$$U^2 \equiv \frac{T_A}{T_\infty} \qquad U_w^2 \equiv \frac{T_{A\,wall}}{T_\infty} \qquad \text{III-(47)}$$

it follows from Eqs III-(40) through III-(47) that

$$N = \frac{2\sqrt{6}\; s\,\delta}{(1 - U_w^2)^s} \int_{U_w}^{1} (U^2 - U_w^2)^{s-1} \left\{ n_{e_\infty} \sigma_{e\text{-}i} + \frac{n_{A_\infty} \sigma_{i\text{-}A}}{U} \right\} dU \qquad \text{III-(48)}$$

For the second iteration we consider a linear variation of temperature with position. This corresponds to setting $s = 1$. While this profile is obviously unrealistic, it provides a demonstration of the sensitivity of the final result to the shape of the heavy-particle temperature profile. Setting $s = 1$ we find

$$(N)_2 = \frac{\sqrt{6}\;\delta}{(1 - T_w/T_\infty)} \left[n_{A_\infty} \sigma_{e\text{-}A} \ln\left(\frac{T_\infty}{T_w}\right) + 2\, n_{e_\infty} \sigma_{e\text{-}i} \left(1 - \sqrt{\frac{T_w}{T_\infty}}\right) \right]$$

Inserting typical values $T_\infty = 12{,}000°K$, $T_w = 300°K$, $n_{A_\infty} = 6 \times 10^{17} cm^{-3}$, $n_{e_\infty} = 2.1 \times 10^{16} cm^{-3}$, $\sigma_{e\text{-}A} = 1.0 \times 10^{16} cm^2$, $\sigma_{e\text{-}i} = 3 \times 10^{-13} cm^2$, and $\delta = 10^{-2} cm$, we find $(N)_2 = 274$

The number of collisions has increased somewhat from the first-approximation value of 163, since we are now considering a mean free path which is smaller than the free-stream value in the regions near $y = o$.

In order to determine the sensitivity to profile, we now set $s = 3$ (approaching a Blasius-like profile) and obtain, as a third iteration,

$$(N)_3 = \frac{6\sqrt{6}\,\delta}{(1-u_w^2)^3}\left[\left\{\frac{1}{4}(1-u_w^4) - u_w^2(1-u_w^2) + u_w^4 \ln\left(\frac{1}{u_w}\right)\right\} M_{e_\infty} G_{e-a}\right.$$

$$\left. + \left\{\frac{1}{5}(1-u_w^5) - \frac{2}{3}u_w^2(1-u_w^3) + u_w^4(1-u_w)\right\} M_{e_\infty} G_{e-i}\right]$$

Evaluating this for the same properties we find $(N)_3 = 187$. Note that these results are consistent with those of Petschek and Byron (32), who obtained about 400 collisions in a boundary layer which was slightly thicker in proportion to the mean free path.

Summarizing, since the energy of the electrons is given by

$$E = \frac{3}{2} k T_e \qquad \text{III-(49)}$$

We have:

<u>First Iteration</u>: Constant λ, Constant T_A

$(N)_1 = 163$, $T_{e\ wall} = 0.996\ T_e$

<u>Second Iteration</u>: Variable λ, Linear variation in T_A

$(N)_2 = 274$, $T_{e\ wall} = 0.993\ T_e$

Third Iteration: Variable λ, Cubic variation in T_A

$(N)_3 = 187$, $T_{e\ wall} = 0.995\ T_e$

From these results we may draw four conclusions:

(1) The electron temperature is very nearly frozen at its free-stream value.

(2) The final electron temperature at the wall is almost independent of the shape of the heavy-particle temperature distribution throughout the boundary layer.

(3) There is no need to use the complicated Blasius profile (which may not even be a priori correct in an ionized gas), since the final result is clearly bounded between $0.993\ T_{e_\infty}$ and $0.996\ T_{e_\infty}$, and the accuracy of the probe itself will be far less than these tiny corrections.

(4) The electron temperature one mean free path from the probe surface, as measured by an electrostatic probe, will reflect the value of the electron temperature in the free plasma within 1%.

Case II. Recombination

We must now consider the validity of the basic assumption of Case I, namely, that a particle (viz. an electron) will not recombine when being drawn through the boundary layer towards a probe with an attracting potential.

From Massey and Burhop (51) the relevant recombination mechanisms in argon are as follows:

A. Radiative Recombination: $A^+ + e^- \rightarrow A^* + h\nu$

B. Dielectronic Recombination: $A^+ + e^- \rightarrow A^{**} \rightarrow A^* + h\nu$

C. Dissociative Recombination: $AA^+ + e^- \rightarrow A^* + A^*$

D. Three-body Recombination: $A^+ + e + X \rightarrow A + \tilde{X}$

where the asterisk $(^*)$ denotes an excited electronic state and the tilde $(\sim)$ denotes excess kinetic energy. The decay scheme from excited states has been shown in terms of photon emission, although this could also occur by a superelastic collision. We shall proceed to consider each of these separately. Our criteria as to the importance of recombination shall be a simple one: Does the characteristic time τ for recombination exceed the transit time t for an electron through the boundary layer? If $\tau \gg t$, the particle will not have sufficient time to recombine. On the other hand, if $\tau \ll t$ recombination will be important. To calculate the electron transit time t_e we write

$$t_e = \sqrt{6} \int_0^{\delta} \frac{dy}{\bar{c}_{drift}} \qquad \text{III-(50)}$$

If we assume ambipolar diffusion in the boundary layer (61),

$$\bar{c}_{drift} = 2\,\bar{c}_i \qquad \text{III-(51)}$$

Using the appropriate numerical values given previously, we find $t_e = 1.3 \times 10^{-7}$ seconds.

To compute the characteristic time for recombination, we note (36,51)

$$\lambda_R = \frac{1}{n_i \sigma_R} \qquad \text{III-(52)}$$

where the subscript R denotes recombination. Further, the recombination coefficient α_R is defined in terms of the rate of recombination (51,58,59):

$$-\frac{dn_e}{dt} = \sigma_R \bar{v}\, n_e n_i \equiv \alpha_R n_e n_i \qquad \text{III-(53)}$$

from which $\alpha_R = \sigma_R \bar{v}$, where $\bar{v}$ is the relative velocity of the colliding species. Since the electrons move at least 271 times as fast as the ions, $\bar{v} \cong \bar{c}_e$

Therefore

$$\alpha_R = \sigma_R \bar{c}_e \qquad \text{III-(54)}$$

Substituting Eq III-(43) into Eq III-(41), we find

$$\lambda_R = \frac{\bar{c}_e}{n_i \alpha_R}$$

Since we may now define the characteristic time for recombination

$$\tau \equiv \lambda_R / \bar{c}_e$$

or $$\tau = 1/n_i \alpha_R \qquad \text{III-(55)}$$

Therefore, the characteristic time for a specific recombination process depends solely upon the value of the product of ion particle density and the recombination coefficient for that particular process. Note that τ is just the inverse of the usual collision frequency.

A. Radiative Recombination:

Massey and Burhop (51) give a value of $3 \times 10^{-19} cm^2$ for the radiative recombination cross section for argon at electron velocities corresponding to room temperatures. Since recombination is less likely at higher electron temperatures, using this value would represent the highest rate of recombination possible.

Thus:

$$\alpha_R = 3 \times 10^{-19} \text{ cm}^2 \times 7 \times 10^7 \text{ cm/sec}$$
$$= 2.1 \times 10^{-11} \text{ cm}^3/\text{sec}$$

and, using the largest value of n_e to get the smallest possible recombination time, we choose $n_e = (n_e)_{wall} = 4.0 \times 10^{16}$ per cm^3. Thus $\tau_{\text{rad. recomb.}} \geq 1.2 \times 10^{-5}$ seconds. Clearly, the characteristic time $\tau \gg t_e$; therefore radiative recombination of the electron with an ion is highly unlikely during the electron's passage to the probe.

B. Dielectronic Recombination:

Massey and Burhop (51), page 632, give the expression

$$\alpha_{\text{die-recomb}} = 10^{-14} \sum_s \frac{\omega_s}{2\omega_s} e^{-E_s/kT} \qquad \text{III-(56)}$$

where E_s is the energy of the doubly-excited S level and ω_s is the degeneracy of that level. Clearly the dielectronic recombination coefficient decreases strongly with increased energy of the doubly-excited configuration with respect to the ground state. That is, it is exponentially more difficult for the recombination process to occur if the electrons must have sufficient energy to produce a high-energy doubly-excited state. Even if these energies are only comparable to kT (in general they will be much higher), then $\alpha \approx 10^{-12} \text{cm}^3/\text{sec}$. In this case

$$\tau_{\text{die. recomb.}} = 2.5 \times 10^{-5} \text{ sec}$$

This is still 250 times as long as the transit time, so we may neglect dielectronic recombination.

C. Three-Body Recombination:

Again, from Massey and Burhop (51), page 635, for argon at N.T.P. with $T_e = 10{,}000°K$, $\alpha_{\text{3-body recomb.}} = 6.8 \times 10^{-11} \times [(300)/10{,}000]^{1/2} \approx 10^{-11}$. Since the recombination coefficient decreases with increased temperature, the choice of N.T.P. conditions will result in the maximum possible recombination rates. From Eq III-(55) we may now calculate that

$$\tau_{\text{3-Body Recomb}} \geq 2.5 \times 10^{-6} \text{ sec.}$$

This is still at least 20 times greater than the residence time of the electrons in the boundary layer.

D. Dissociative Recombination:

At present there are very few data available concerning the process of dissociative recombination. In the main regions of the plasma, which are near equilibrium, detailed balancing must apply. This means that if dissociative recombination is to be the dominant method of electron-positive ion recombination according to the relation

$$AA^+ + e^- \rightarrow A + \tilde{A} \qquad \text{III-(57)}$$

then the inverse process

$$A + \tilde{A} \rightarrow AA^+ + e, \qquad \text{III-(58)}$$

"associative ionization", must be the dominant ionization mechanism. However, in a region of nonequilibrium such as that near the probe, Eq III-(58) need not follow as a consequence of Eq III-(57). Nonetheless it is still reasonable to assume that the recombination rate due to dissociative recombination does not exceed the rate of recombination due to three-body recombination. Assuming this to be true, we are led to the important conclusion that the probability of an electron recombining during its passage through the boundary layer surrounding a cooled electrostatic probe is very small. Therefore, the calculations based upon the assumption of no recombination (Case I) should be substantially correct.

Case III. The Strongly Negative Probe Problem:

In Case I we discussed the situation appropriate to the collection of electrons by a positively charged probe. We now consider the inverse problem; namely, the collection of positive ions by a strongly negative probe.

From our previous analysis [(Eq III-(55)] we have shown that the characteristic time for recombination depends solely upon the product of the particle density of the target species and the recombination coefficient for the particular process. Since the recombination coefficient makes no distinction as to whether the electron strikes the ion or vice-versa, this quantity will remain the same. Thus, the characteristic time for recombination is the same as in Case II. This is easily understood, since it implies that the microscopic

recombination process does not depend upon how we identify the "target" and the "projectile" particles.

However, our basic criterion for recombination was the relative magnitudes of the recombination time and the transit time. For ions instead of electrons, in the case of ambipolar diffusion, Eq III-(50) integrates to the form

$$t_i = \frac{\sqrt{6}}{2} \frac{\delta}{\bar{c}_i} \qquad \text{III-(59)}$$

However, we have seen previously that $\bar{c}_i = 2.5 \times 10^5$ cm/sec, from which $t_i = 1.3\ 10^{-7}$ sec. Comparison of this with the characteristic recombination times shows that for the ions and the electrons

$$\tau \approx 20\, t \qquad \text{III-(60)}$$

Physically, this implies that ions and electrons can be collected by an electrostatic probe, since their transit times through the boundary layer are significantly smaller than the recombination time.

In summary, therefore, we conclude that the boundary layer must be considered a nonequilibrium region. This is so for the following reasons:

(a) The electron temperature is approximately constant throughout the boundary layer due to the insufficient transfer of energy by collisions of the electrons with the heavy particles.

(b) The heavy particle temperature decreases sharply in the boundary layer. Therefore, in the boundary layer, $T_e > T_H$ and thermal equilibrium does not hold.

(c) Assuming the perfect gas law holds for each component, then $p_e = n_e kT_e$ and $p_i = n_i kT_i$. Since $T_e > T_i$ and $n_e = n_i$ in the boundary layer, then $p_e > p_i$. Hence the partial pressure of the electrons is greater than the partial pressure of the ions, even though both species are present in the same numbers per unit volume.

D. DISCUSSION

The theory for plasma diagnosis by use of a cooled electrostatic probe leads to the series of conclusions listed below. These conclusions are, in part at least, confirmed by the initial experimental data shown in Figure 21. The data were not reduced to determine an electron temperature because the insulator used to isolate a small section of probe surface surface ablated away with time. Thus the data of Figure 21, while qualitatively significant, are probably not quantitatively accurate. Experiments are now in progress using an improved probe with a more suitable insulator.

The following conclusions have been made:

(1) The hydrodynamic effects of the probe are confined solely to the boundary layer region, since the transition region is only the order of a mean free path thick.

(2) Weak-field effects due to the potential of the probe relative to that of the neutral plasma extend about 1/3 electron-ion mean free path beyond the sheath. This "transition region" is about 0.01 of the boundary layer thickness.

(3) Strong-field effects are confined to the sheath proper. This is about 0.05 of the transition region.

(4) The electrons suffer sufficiently few collisions in migrating across the boundary layer and transition region that their temperature in the vicinity of the probe is within a percent of their temperature in the neutral plasma.

(5) The probability is very small that an electron or an ion will suffer a recombination collision within the boundary layer.

(6) For a Langmuir probe $(j_e)_{sat}/(j_i)_{sat} = \mp(m_e/m_i)$ and $\Phi_F = \Phi_F(m_e/m_i, T_e)$. For an electrostatic probe in a dense plasma $(j_e)_{sat}/(j_i)_{sat} = \mp(m_e/m_i, T_{e\infty}, T_{A\ wall})$ and $\Phi_F = \Phi_F(m_e/m_i, T_{e\infty}, T_{A\ wall})$.

(7) Since the sheath is very much smaller than the radius of the probe the collection of current by an electrostatic probe in a dense plasma is negligibly influenced by the actual geometry of the probe. In short, the probe acts as if it were planar.

(8) The electron particle density at the probe surface is significantly changed from its free stream value. However, the function relating these quantities depends solely upon conditions at the probe and in the free stream and is totally independent of the nature of the variations within the boundary layer.

(9) The result concerning the constancy of the electron temperature through the boundary layer is quite insensitive to the nature of the heavy-particle temperature profile in the boundary layer.

(10) Provided the electron energy distribution is Maxwellian, the slope of the semi-logarithmic plot of current versus voltage should give an accurate estimate of the electron temperature, regardless of end effects or orbital motions due to the very weak induced magnetic fields.

It is important to note that the use of an electrostatic probe in a dense plasma, as analyzed above, does not violate Langmuir's original statement, "An electrostatic probe is possible only when the probe diameter is much smaller than the mean free path". However, it is necessary to apply the proper interpretation to this statement.

The original theory for the use of an electrostatic probe (37,39,40, etc.,) was derived on the assumption

$$\frac{L}{\lambda} \ll 1 \qquad \text{III-(61)}$$

where λ is the relevant mean free path and L is a characteristic length.

This concept presupposes that the boundary layer resulting when Eq III-(61) is not satisfied will sufficiently distort the free-stream electron conditions to render measurement of electron temperature meaningless.

However, in reality the criterion is really a double one. In order to be able to measure <u>ionic</u> phenomena (i.e., ion temperature), Eq III-(61) is the correct criterion. But in order to measure the <u>electronic</u> phenomena (i.e., electron temperature, electron random current density, electron particle density and plasma potential), the following criterion is proper

$$\beta \equiv 2\sqrt{6}\ \frac{m_e}{m_i}\ \frac{\delta}{\lambda} \ll 1 \qquad \text{III-(62)}$$

Physically, Eq III-(61) implies that the ions shall not lose much energy in travelling to the probe (i.e., their mean free path is large, and so they fall into the probe without suffering many collisions). Similarly, Eq III-(62) implies that the electrons shall not lose much energy in traversing the boundary layer thickness δ.

Note that Eq III-(62) is not nearly so severe a requirement as Eq III-(61). For a typical case of interest, e.g., an argon plasma at one atmosphere pressure and 12,000°K, $L/\lambda \approx 1000$, where L = length of cylindrical probe surface exposed to the plasma. Clearly this does not satisfy Eq III-(61), and hence no information can be gathered, since the ion temperature is so severely distorted by the boundary layer. However, for argon $m_e/m_i = 1/72{,}000$, and for the case of interest ($\delta = 0.01$ cm)

$$\beta \approx \frac{1}{200}$$

which <u>does</u> satisfy Eq III-(62), indicating that <u>electronic</u> information can be gathered under these circumstances.

Therefore the "classic" statement, "An electrostatic probe is possible only when the probe diameter is much smaller than the mean free path," is applicable to ions in a dense plasma, but does not apply to the electrons.

A further significant departure from classical Langmuir probe theory concerns the ratio of saturation currents. The classical result predicts $(j_e)_{sat} = \sqrt{\frac{m_i}{m_e}}\ (j_i)_{sat}$, a result which is independent of boundary layer effects. However,

from Eq III-(9) we find that for a cooled electrostatic probe in a dense plasma

$$\frac{(j_e)_{SAT}}{(j_i)_{SAT}} = \sqrt{\frac{m_i}{m_e}} \left(\frac{T_{e\infty}}{T_{A\,WALL}}\right)^{1/2} \qquad \text{III-(63)}$$

neglecting variations in the heavy particle temperature over the last mean free path. This is clearly greater than the Langmuir result, since $T_{e_\infty} > T_{A\ wall}$. Over the range of interest this ratio, instead of taking the classical value of 271 (for argon), varies from 700-2000 depending upon the local value of T_{e_∞}.

IV. CONCLUSIONS

1. The most significant process in the mixing of a laminar argon arcjet with stagnant helium was found to be the flow of helium into the jet. The effects of ionization, radiation, and jet dispersion were theoretically and experimentally shown to be negligible. This results from helium's high heat capacity and diffusion coefficient at arcjet temperatures.

2. A theoretical model for laminar mixing of an argon arcjet in stagnant cold helium has been established on the basis of boundary-layer-type assumptions and transport properties computed by the Chapman-Enskog techniques. Electron-heavy-particle equilibrium was assumed. The good general agreement between theory and experiment shows that these assumptions were valid for the case studied.

3. A water-cooled electrostatic probe has been shown analytically to be useful for measuring electron energy and density in a dense plasma, because although the probe will cool the heavy particles in its neighborhood, the electrons remain essentially unaffected. Measurements of electron currents as a function of probe voltage can then be made in a manner similar to that of classical Langmuir probe technique. A preliminary qualitative experiment has confirmed the general nature of the predicted behavior.

V. REFERENCES

1. Grey, J., Williams, P. M., Sherman, M. P., and Jacobs P. F., "Laminar Mixing and Heat Transfer Phenomena Between a Partially Ionized Gas and a Gaseous Coolant," Report No. ARL 63-237, OAR, USAF, December, 1963.

2. Grey, J., Jacobs, P. F., "Experiments on Turbulent Mixing in a Partially Ionized Gas," AIAA Journal, Vol. 2, March, 1964, pp. 433-438.

3. Grey, J., Sherman, M. P., and Jacobs, P. F., "Analytical Experimental Correlation of Radiation Loss from an Argon Arcjet," Princeton University Aeronautical Engineering Laboratory Report No. 658, July, 1963.

4. Grey, J., Jacobs, P. F., and Sherman, M. P., "Calorimetric Probe for the Measurement of Extremely High Temperatures," Rev. Sci. Instr., 33, July 1962, pp. 738-741.

5. Grey, J., Sherman, M. P., Jacobs, P. F., "Measurements of Arcjet Radiation with a Cooled Collimated Probe," IEEE Transactions on Nuclear Science, Vol. NS-11, January, 1964, p. 176.

6. Grey, J., and Jacobs, P. F., "Turbulent Mixing in a Partly Ionized Gas," Princeton University Aeronautical Engineering Laboratory Report No. 625, September, 1962.

7. Sherman, M. P., Grey, J., and Jacobs, P. F., "The Degree of Approach to Equilibrium in an Atmospheric-Pressure Arcjet Using Argon," Princeton University Aeronautical Engineering Laboratory Report No. 645, April, 1963, (Revised October, 1964).

8. Sherman, M. P., "Calculation of Transport Properties of Mixtures of Helium and Partly-Ionized Argon," Princeton University Aeronautical Engineering Laboratory Report No. 673, December, 1963.

9. Grey, J., Williams, P. M., Fradkin, D. B., "Mixing and Heat Transfer of an Argon Arcjet with a Coaxial Flow of Cold Helium," Princeton University Aeronautical Engineering Laboratory Report No. 710, November, 1964.

10. John, R. R., Bennett, S., and Connors, J., "Experimental Performance of a High Specific Impulse Arc Jet Engine," Fourth Electric Propulsion Conference, Philadelphia, Pa., August, 1964, AIAA Paper 64-669.

11. Sherman, M. P., and Grey, J., "Interactions Between a Partly-Ionized Laminar Subsonic Jet and a Cool Stagnant Gas," Princeton University Aeronautical Engineering Laboratory Report No. 707, September, 1964.

12. Squire, H. B., "The Round Laminar Jet," Quarterly Journal of Mechanics and Applied Math., Vol. 4, September, 1951, p. 121.

13. Schlichting, H., "Laminae Stahlausbreitung", ZAMM Vol. 13, p. 260, 1933 (Boundary Layer Theory, Schlichting, H., McGraw-Hill 1960).

14. Bickley, W., "The Plane Jet," Phil. Mag. Ser. 7, Vol. 23, p. 727, 1939.

15. Toose, D. G., "The Laminar Motion of a Plane Symmetrical Jet of Compressible Fluid," Quart. Journal of Mechanics and Applied Math, Vol. 5, 1952, p. 155.

16. Pack, D. C., "Laminar Flow in an Axially Symmetric Jet of Compressible Fluid, Far from the Orifice," Proc. Camb. Phil. Soc., Vol. 30, 1954, p. 98.

17. Crane, L. J., and Pack, D. C., "The Mixing of a Jet of Gas with an Atmosphere of a Different Gas at Large Distances from the Orifice," Quart. Journal Mechanics and Applied Math, Vol. 14, 1961, p. 385.

18. Kleinstein, G., "An Approximate Solution of the Axisymmetric Jet of a Laminar Compressible Fluid," Quart. of Applied Math, Vol. 20, 1961, p. 49.

19. Pai, S. I., "Two-Dimensional Jet Mixing of a Compressible Fluid," Journal of Aero. Sci., Vol. 16, 1949, p. 463.

20. Pai, S. I., "Axially Symmetric Jet Mixing of a Compressible Fluid," Quart. of Applied Math, Vol. 10, July, 1952, p. 141.

21. Adamson Jr., T. C., "Ignition and Combustion in a Laminar Mixing Zone," Jet Propulsion Lab., C.I.T., Report No. 20-79, 1954.

22. Kovitz, A. A., "Ignition in the Laminar Wake of a Flat Plate," Ph.D. Dissertation, Princeton University, 1956.

23. Kovitz, A. A., "Laminar Parallel Stream Mixing with Dissociation and Recombination," Ph. of Fluids, Vol. 3, 1960, p. 436.

24. Weinstein, H., and Todd, C. A., "A Numerical Solution of Mixing of Laminar Coaxial Streams of Greatly Different Densities-Isothermal Case," NASA TN D-1534, February, 1963.

25. Chapman, S., and Cowling, T. G., "Mathematical Theory of Non-Uniform Gases," 1939, 1952, Cambridge University Press.

26. Hirschfelder, J. O., Curtiss, C. F., and Bird, R. B., "Molecular Theory of Gases and Liquid," 1954, McGraw-Hill.

27. Pai, S. I., Fluid Dynamics of Jets, D. van Nostrand Company, Princeton, New Jersey, 1954.

28. Finkelnburg, W., and Maecker, H., "Electrische Bogen and Thermisches Plasma," Encyclopedia of Physics, Vol. xxii, p. 254.

29. Amdur, I., and Mason, E. A., "Properties of Gases at Very High Temperatures," Physics of Fluids, Vol. 1, September-October, 1958, p. 370.

30. Cohen, R. S., Spitzer, L., and Routly, P. M., "The Electrical Conductivity of an Ionized Gas," Phy. Rev., Vol. 30, October, 1950, p. 230.

31. Robinson, B. B., and Bernstein, I. B., "A Variational Description of Transport Phenomena in a Plasma," Princeton University Plasma Physics Laboratory Report MATT-65, April, 1961.

32. Petschek, H. and Byron, H., "Approach to Equilibrium Ionization behind Strong Schock Waves in Argon," ANNALS of Physics, Vol. 1, 1957, pp. 270-315.

33. Kahalas, S. L., and Kashian, H. C., "On the Approach of Electrons to Equilibrium," Physics of Fluids, Vol.2, No. 2, March, 1959, pp. 100-102.

34. Pyette, A., and Williams, A. R., "On Electrical Conduction in a Non-Uniform Helium Plasma," ARL 63-166, September, 1963.

35. Cahn, J. H., "Electronic Interaction in Electrical Discharges in Gases," Physical Review, Vol. 75, No. 2, January, 1949, pp. 293-300.

36. Glasstone, S., and Lovberg, R. H., "Controlled Thermonuclear Reactions," (D. Van Nostrand Company, Princeton New Jersey, 1960), pp. 179-202.

37. Langmuir, I., and Mott-Smith, H., "Studies of Electric Discharges in Gases at Low Pressures," General Electric Review, Vol. 27, Numbers 7, 8, 9, 11 and 12, 1924, pp. 449-455, 538-548, 616-623, 762-771 and 810-820.

38. Mott-Smith, H. M., and Langmuir, I., "The Theory of Collectors in Gaseous Discharges," Physical Review, Vol. 28, October, 1926, pp. 727-763.

39. Langmuir, I., "The Interaction of Electron and Positive Ion Space Charges in Cathode Sheaths," Physical Review, Vol. 33, June, 1929, pp. 954-990.

40. Tonks, L., and Langmuir, I., "A General Theory of the Plasma of an Arc," Physical Review, Vol. 34, September, 1929, pp. 876-922.

41. Boyd, R. L. F., "The Collection of Positive Ions by a Probe in an Electrical Discharge. Proc. Roy. Soc. London, Vol. 201-A, pp. 329-347, 1950.

42. Boyd, R. L. F., and Twiddy, N. D., "Electron Energy Distribution in Plasmas," Proc. Roy. Soc. London, Vol. 250-A, 1955, pp. 53-69.

43. Allen, J. E., Boyd, R. L. F., and Reynolds, P., "The Collection of Positive Ions by a Probe Immersed in a Plasma," Proc. Phys. Soc. London, Series B, Vol. 70, 1957, pp. 297-304.

44. Bernstein, I. B., and Rabinowitz, I. N., "Theory of Electrostatic Probes in a Low-Density Plasma". Physics of Fluids, Vol. 2, No. 2, March-April, 1959.

45. Cohen, I. M., "Asymptotic Theory of Spherical Electrostatic Probes in a Slightly Ionized, Collision-Dominated Gas". Physics of Fluids, Vol. 6, No. 10, October, 1963, pp. 1492-1499.

46. Chen, F. F., "Use of Electrostatic Probes in Plasma Physics," Princeton University, MATT 184, February, 1962.

47. Gardner, A. L., Barr, W. L., Kelly, R. L., and Oleson, N.L., "Diagnostic Measurements on a Highly Ionized, Steady-State Plasma," Physics of Fluids, Vol. 5, No. 7, July, 1962, pp. 794-802.

48. Hall, L. S., "Probes and Magnetic Pumping in Plasma" (Ph.D. Thesis), Lawrence Radiation Laboratory, U.C.R.L. 6535, July, 1961.

49. Su, C. H., and Lam, S. H., "Continuum Theory of Spherical Electrostatic Probes," Physics of Fluids, Vol. 6, No. 10, October, 1963, pp. 1479-1491.

50. Talbot, L., "Theory of the Stagnation-Point Langmuir Probe," Physics of Fluids, Vol. 3, No. 2, March, 1960, pp. 289-297.

51. Massey, H. S. W., and Burhop, E. H. S., "Electronic and Ionic Impact Phenomena," (Oxford University Press, 1951) pp. 618-641.

52. Spitzer, L., "The Physics of Fully Ionized Gases," (Interscience Publishers, London, 1956).

53. Delcroix, J. L., "Introduction to the Theory of Ionized Gases," (Interscience Publishers, New York, 1960).

54. Cobine, J. D., "Gaseous Conductors," (Dover Publications Inc., New York, 1958).

55. Harwell, K. E., and Jahn, R. G., "Initial Ionization Rates in Shock-Heated Argon, Krypton and Xenon," Physics of Fluids, Vol. 7, No. 2, February, 1964, pp. 214-222.

56. Dällenbach, W., "Mixed Sustained and Self-Sustained Discharge Mechanism in Shock-Ionized Argon," Physics of Fluids, Vol. 7, No. 1, January, 1964, pp. 138-141.

57. Dewan, E. M., "Generalizations of the Saha Equation," Physics of Fluids, Vol. 4, No. 6., June, 1961, pp. 759-764.

58. Schlichting, H.,"Boundary Layer Theory," (Pergamon Press Ltd., 1955), translated by J. Kestin, pp. 282-288.

59. Biondi, M. A., and Brown, S. C., "Measurement of Electron-Ion Recombination," Physical Review, Vol. 76, No. 11, December, 1949, pp. 1697-1700.

60. Hinnov, E., and Hirshberg, J. G., "Electron-Ion Recombination in Dense Plasmas," Physical Review, Vol. 125, No. 3, February, 1962, pp. 795-801.

61. Waymouth, J. F., "Perturbations of a Plasma by a Probe," Physics of Fluids, Vol. 7, No. 11, November 1964, pp. 1843-1854.

APPENDIX A

List of Symbols

A_p	Probe surface area, cm^2
b	Charged particle mobility, $\frac{cm/volt}{sec/cm}$
$\vec{\bar{c}}$	Average particle velocity, cm/sec
$\vec{c}_i$	Velocity of particle of species i, cm/sec
$\overline{\vec{c}_i}$	Mean velocity of species i, cm/sec
c_o	Mass average velocity of the center of gravity of a fluid element, cm/sec
c_p	Specific heat at constant pressure, erg/gm-°K
d	Thickness of transition region, cm. Also mean interparticle distance, cm. Also potential coefficient (E.V.-Angstroms)
$\vec{d}_i$	Sum of concentration, pressure, and body forces, "diffusive forces"
D_{i_j}	Mixture diffusion coefficient, cm^2/sec
D_i^T	Thermal diffusion coefficient, gm/cm-sec
D_{i_j}	Binary diffusion coefficient, cm^2/sec
e	Electron charge, 4.8×10^{-10} esu
$\vec{\mathcal{E}}$	Electric field, statvolts/cm
E	Electron energy, erg or E.V. as noted
ΔE	Change in electron energy, erg
f_i	Velocity distribution function of species i normalized to one, $cm^{-3}(cm/sec)^{-3}$
$\bar{F}(\chi)$	Average steric factor
F_i	Body force per particle of species i, dynes

h	Debye length, cm
h	Total enthalpy, cal/gm
I	Current, amperes, also ionization energy (argon) per electron (15.75 ev)
$\overline{\overline{I}}$	Unit tensor
J	Current density, amperes/cm^2
k	Boltzmann constant (1.38×10^{-16} erg/°K)
K_i^*	Rate of production of particles of species i, $(cm^3 - sec)^{-1}$
L	Characteristic length, cm
m	Particle mass, gms
M_i	Molecular weight of species i
M	Average molecular weight
n	Particle density, number/cm^3
N	Number of electron - heavy particle collisions
N_{K_N}	Knudsen Number = λ/L
p	Scalar pressure, dynes/cm^2
$\bar{P}_o$	Impact parameter to give $\frac{\Pi}{2}$ deflection in orbital plane
p^*	Total pressure, dynes/cm^2
$\overline{\overline{P}}$	Pressure tensor, dynes/cm^2
P_{rad}	Radiant power emitted per unit volume, erg/cm^3-sec
Pr	Prandtl number, $\mu c_p/\lambda$
q	Conductive heat flux vector, erg/cm^2-sec
q^*_{rad}	Radiative heat flux vector, erg/cm^2-sec
r	Radial coordinate, cm
R	Ratio of helium to argon atom mass, 0.1002

Re	Reynolds number = $\rho_\infty u_\infty r_n / \mu_\infty$
$\vec{\vec{S}}$	Stress tensor, sec^{-1}
Sc	Schmidt number = $\mu_\infty / \mathcal{D}_\infty \rho_\infty$
S	Surface area, cm^2
t_e	Electron transit time, seconds
T	Temperature, °K
u	Axial velocity component, cm/sec
v_r	Radial velocity component, cm/sec
V	Particle drift velocity, cm/sec
$\bar{v}$	Relative velocity of colliding particles, cm/sec
v	Electric potential, volts
w_i	Mass fraction of species i
x	axial coordinate, cm
X_i	mole fraction of species i
$\bar{X}$	$\equiv X_A + R X_M + X_e$
y	Distance from electrostatic probe, cm
Z	Particle charge in units of proton charge
α	Fraction of electron energy lost per electron-heavy particle collision. Also thermal diffusion factor (See Eq II-31)
β	Electrostatic probe operating criterion
δ	Aerodynamic boundary layer thickness, cm
λ	Thermal conductivity. Also mean free path
Λ	Ratio of Debye shielding distance to $\bar{p}_\infty$
μ	Coefficient of viscosity
ξ	$\equiv y/\delta$

ρ Mass density, gm/cm^3. Also charge density

ρ_i Mass density of species i, gm/cm^3

σ Cross section, cm^2/particle

τ Characteristic time for recombination, seconds

Φ_f Potential at which total probe current is zero, volts

Φ Viscous dissipation, erg/cm^3-sec

χ Deflection angle

Ψ Stream function

ω Degeneracy of doubly excited S level

Subscripts

e Electron

f Final condition

H Heavy particle. Also helium

i Species i, also ion

j Species j

N Number of electron-heavy particle collisions

O Initial conditions

R Random value at a point where the plasma potential is zero

∞ Free stream

Superscripts

* indicates dimensional (as opposed to nondimensional) variable, also indicates excited electronic state

~ indicates excess kinetic energy

T indicates thermal diffusion

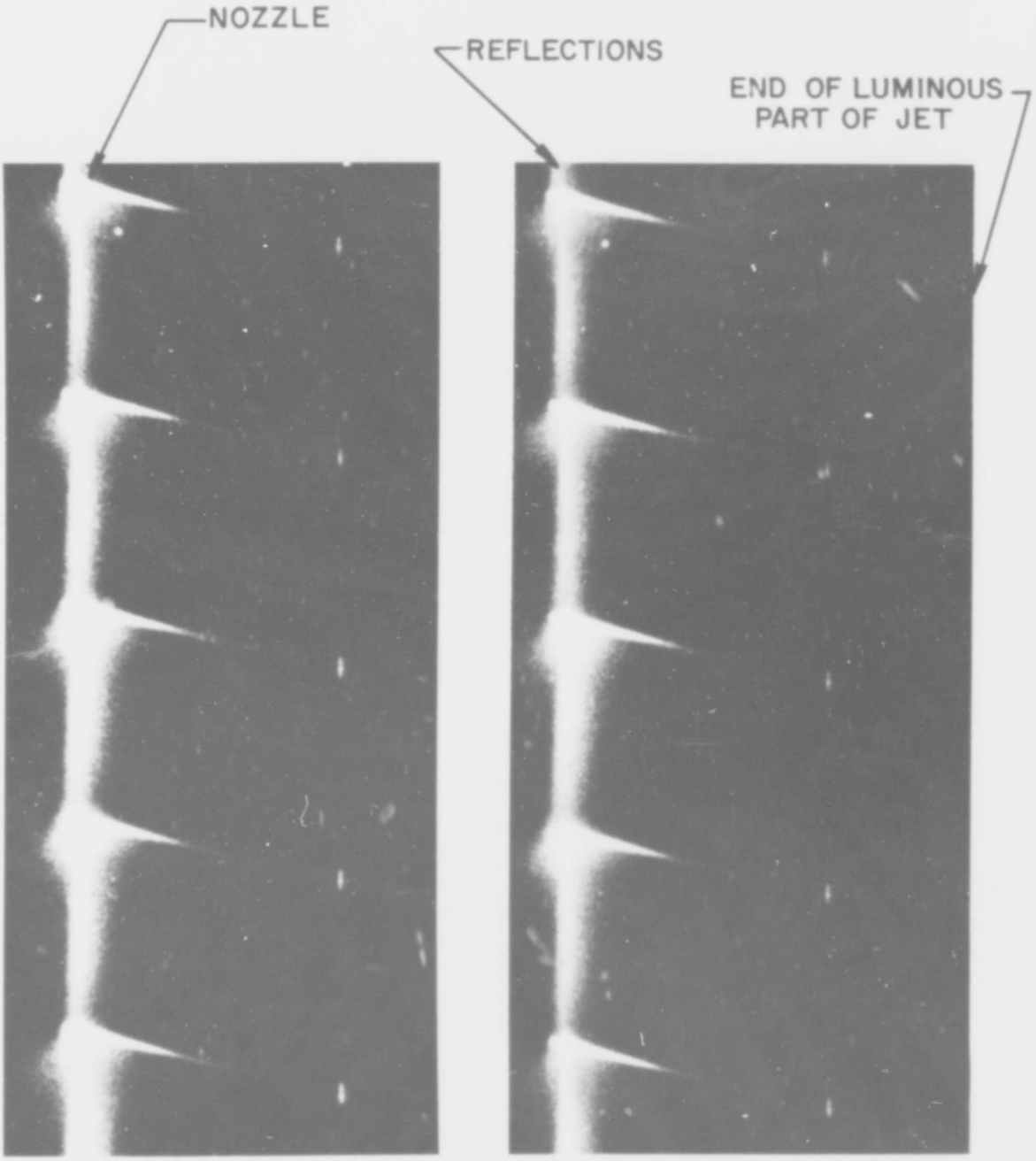

SUCCESSIVE FRAMES OF HIGH SPEED MOTION PICTURES
OF THE LAMINAR ARGON PLASMA JET IN AIR
10,000 FRAMES PER SECOND

FIGURE 1

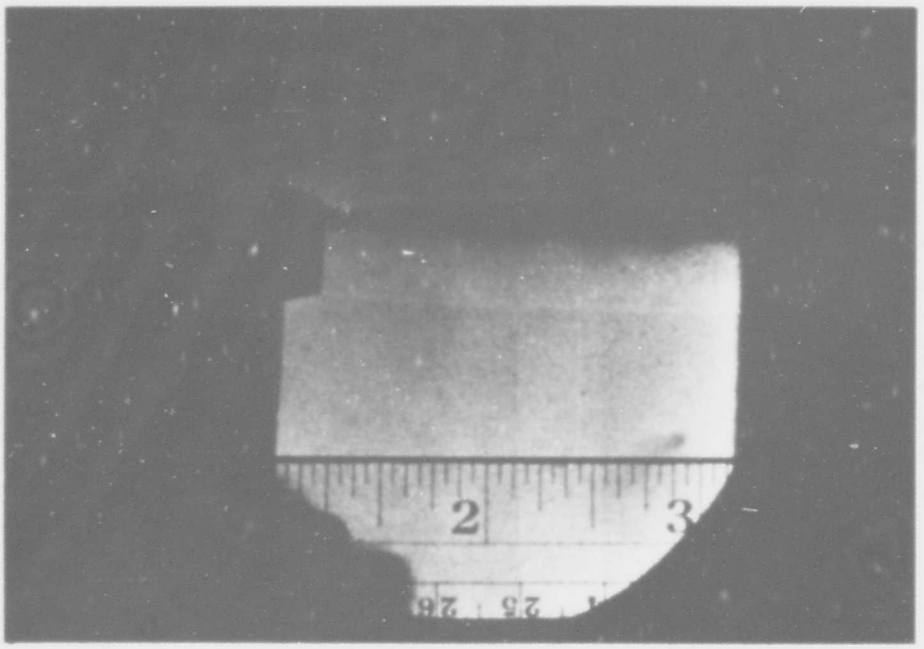

LAMINAR

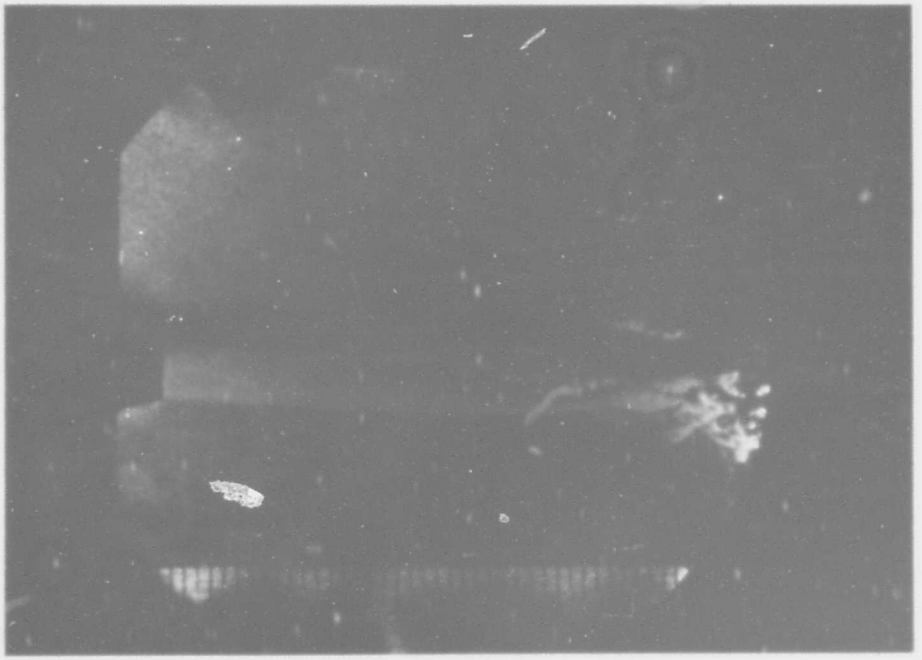

LAMINAR AND TRANSITION

SCHLIEREN PHOTOGRAPHS OF A FREE ARGON ARCJET IN NITROGEN

FIGURE 2

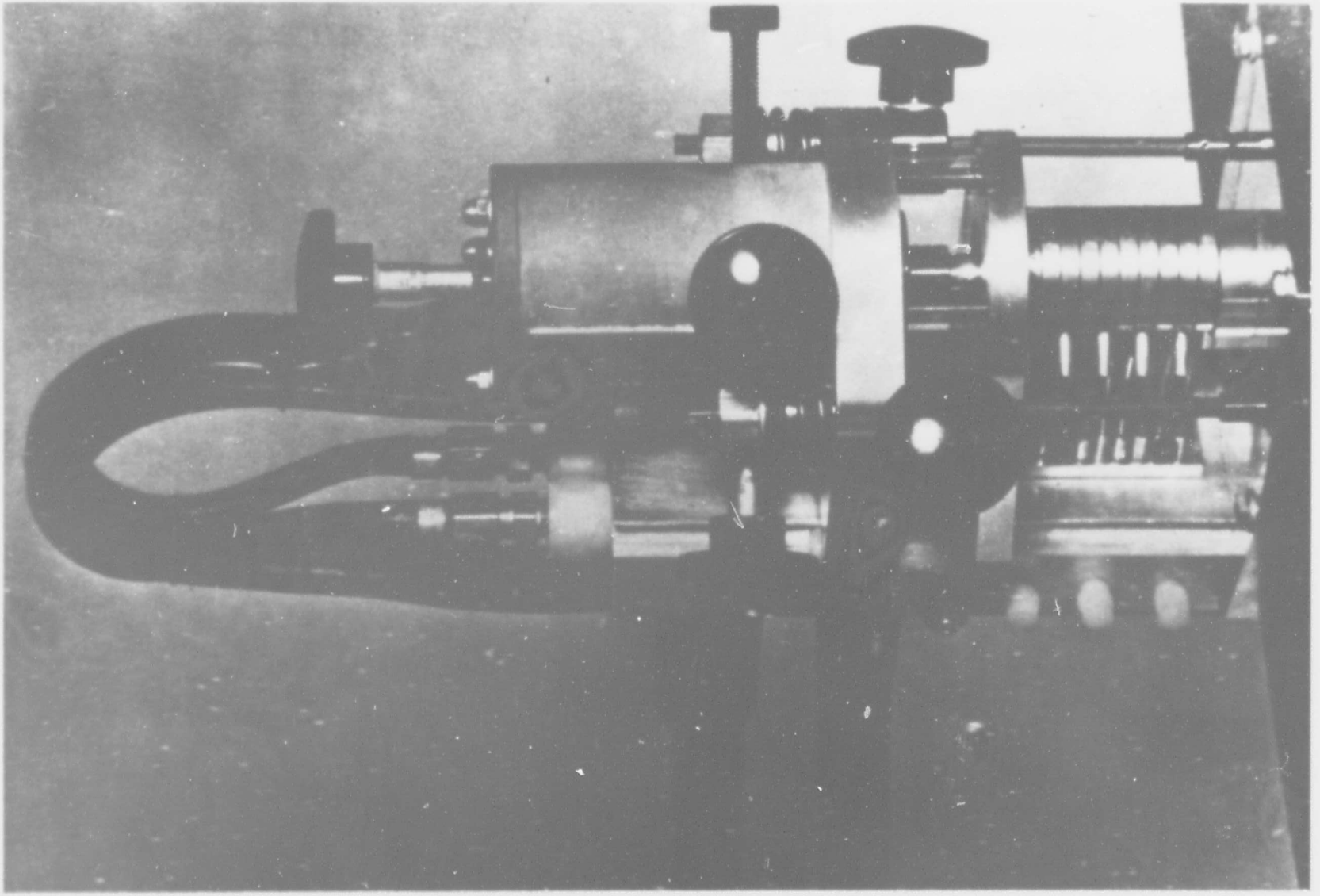

CREARE PLASMA GENERATOR

FIGURE 3

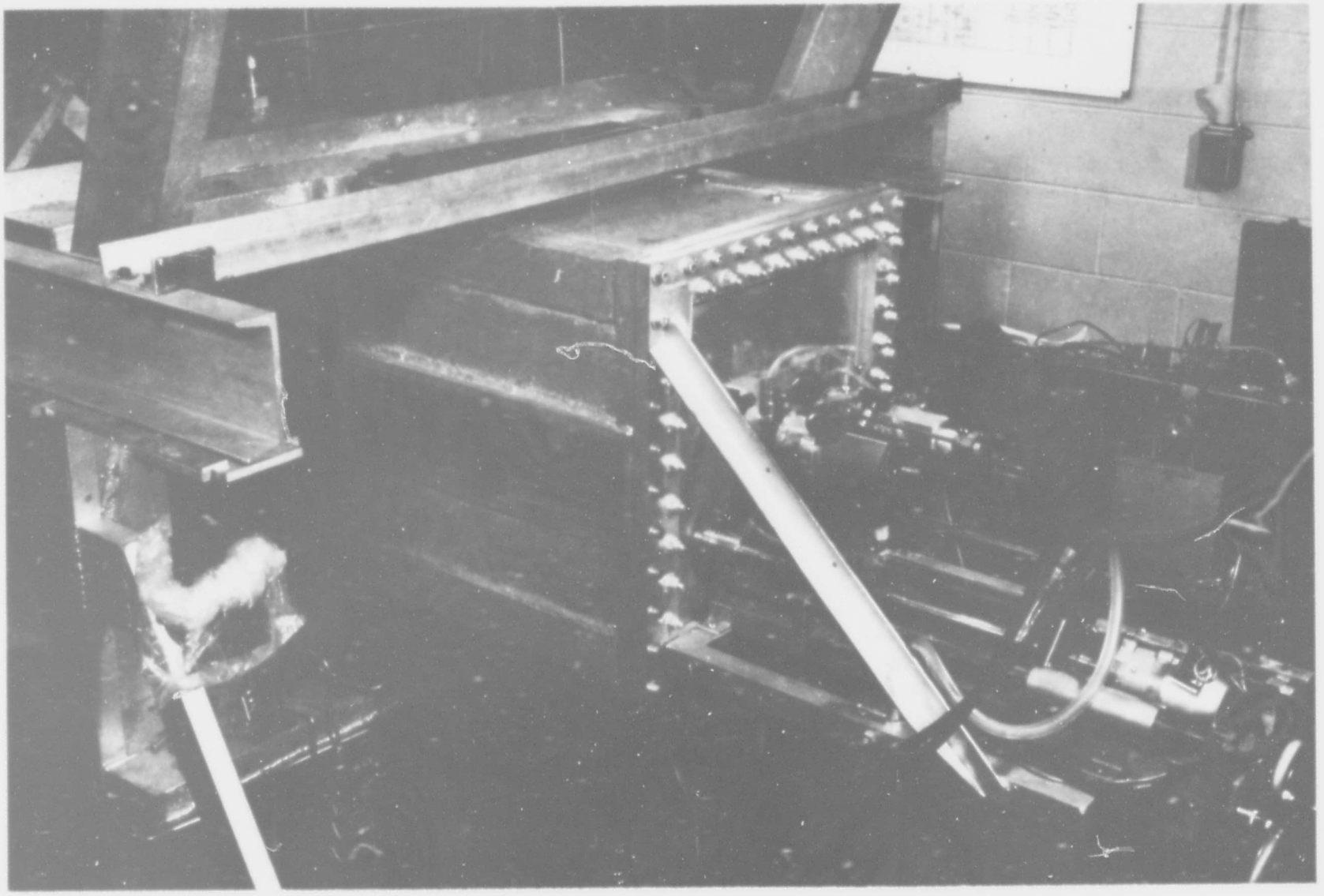

FIGURE 4

CREARE GENERATOR INSTALLED IN TEST APPARATUS

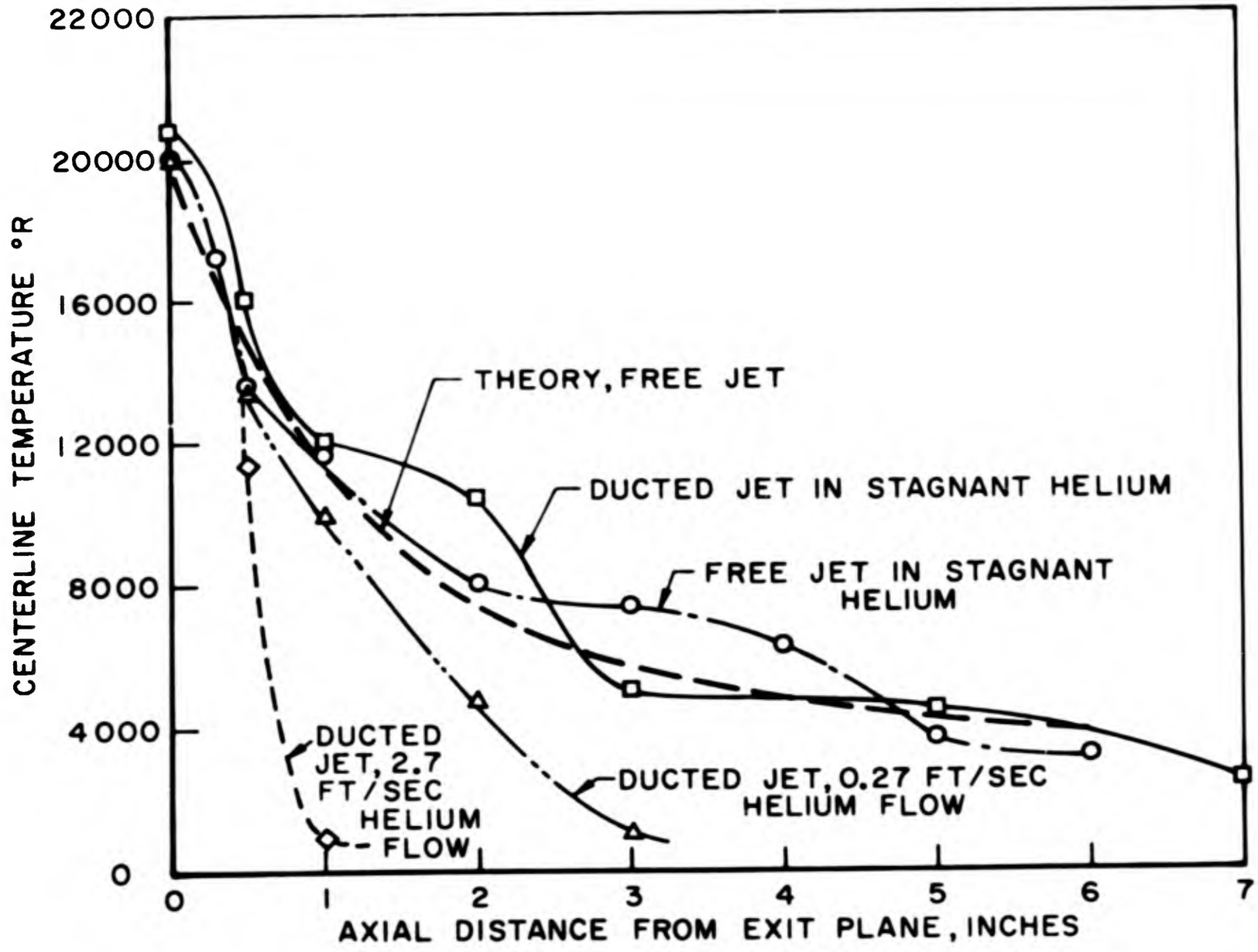

FIGURE 5 CENTERLINE TEMPERATURES VERSUS AXIAL POSITION

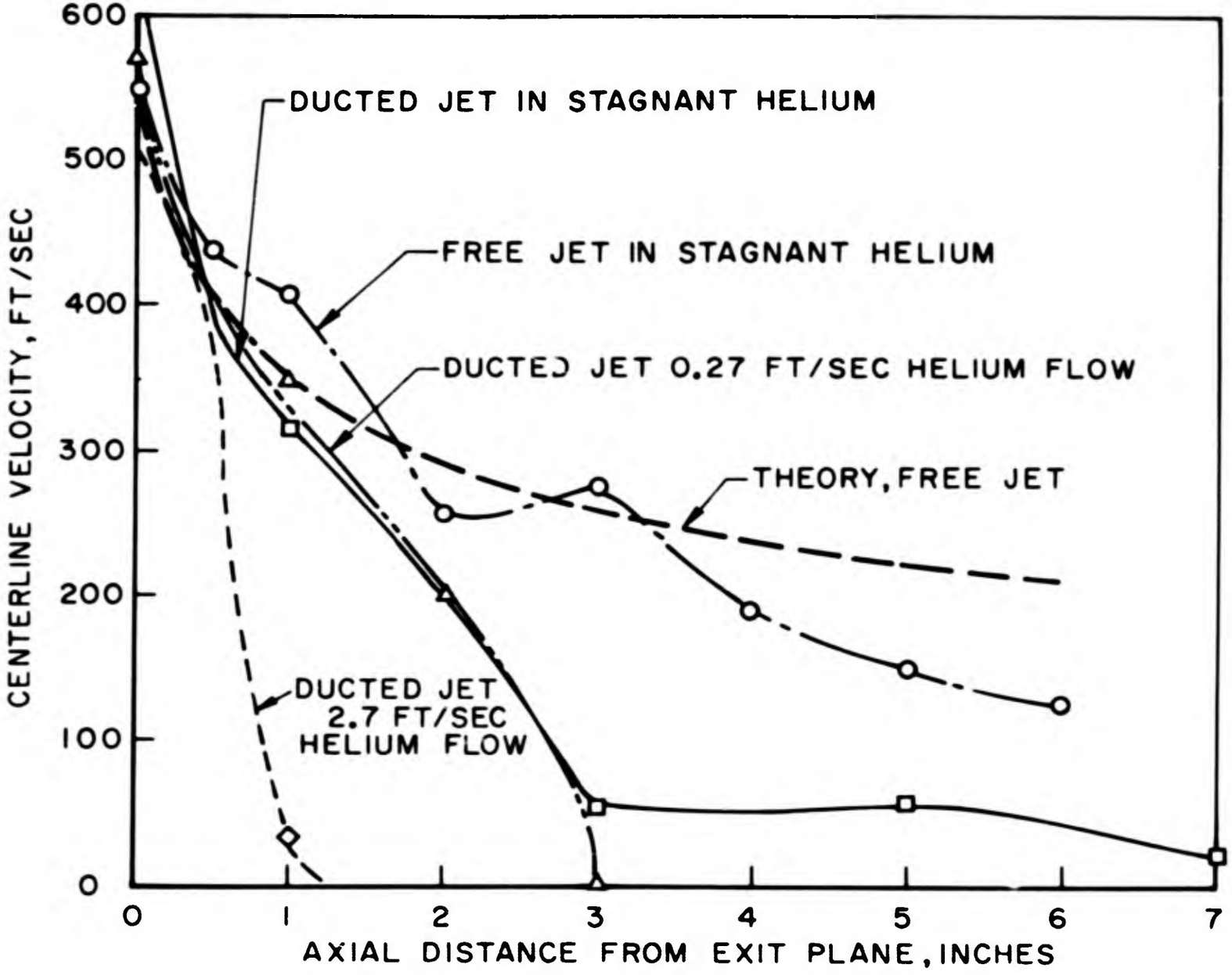

FIGURE 6 CENTERLINE VELOCITIES VERSUS AXIAL POSITION

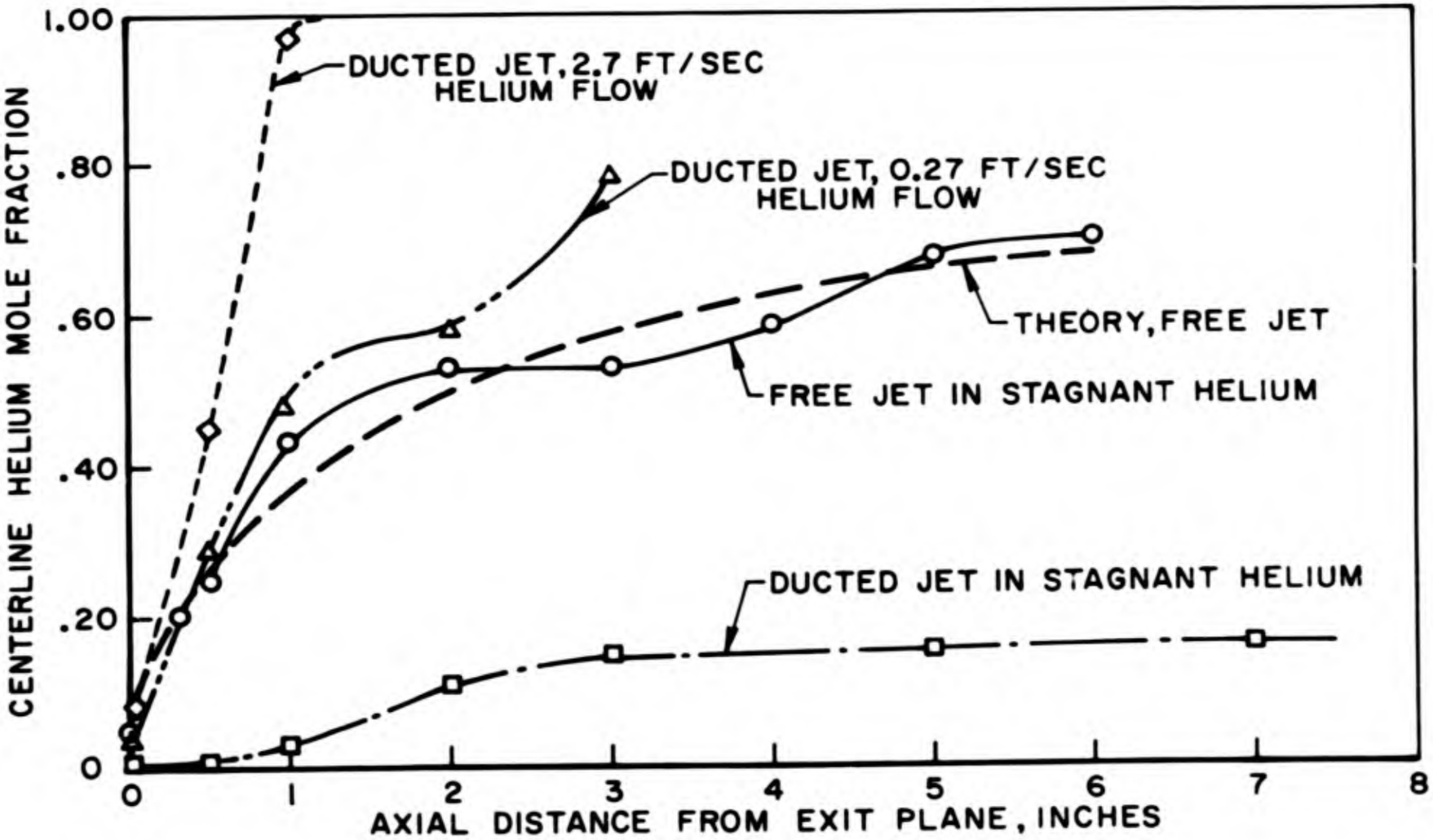

FIGURE 7

CENTERLINE HELIUM CONCENTRATION VERSUS AXIAL POSITION

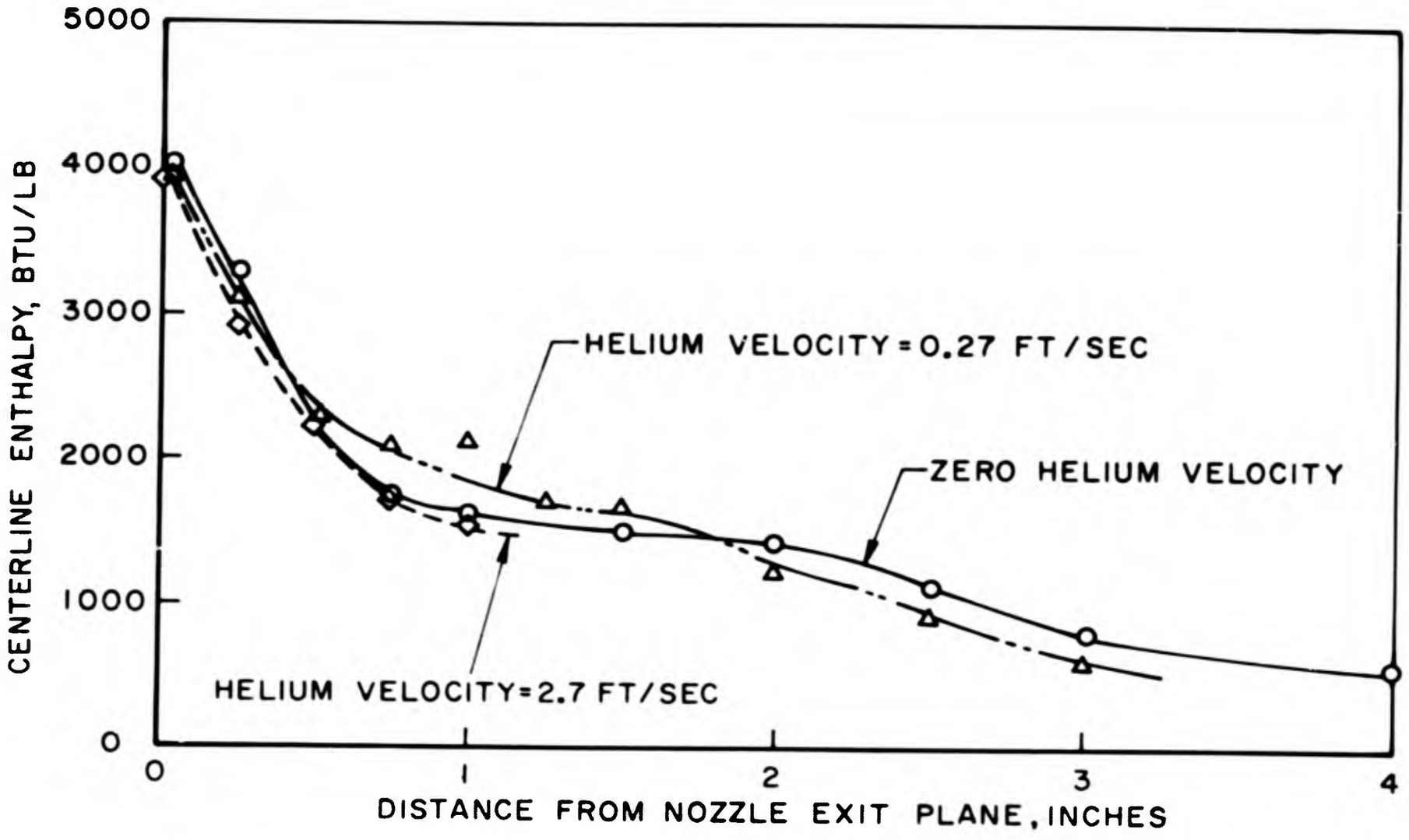

FIGURE 8

CENTERLINE ENTHALPY VERSUS AXIAL POSITION

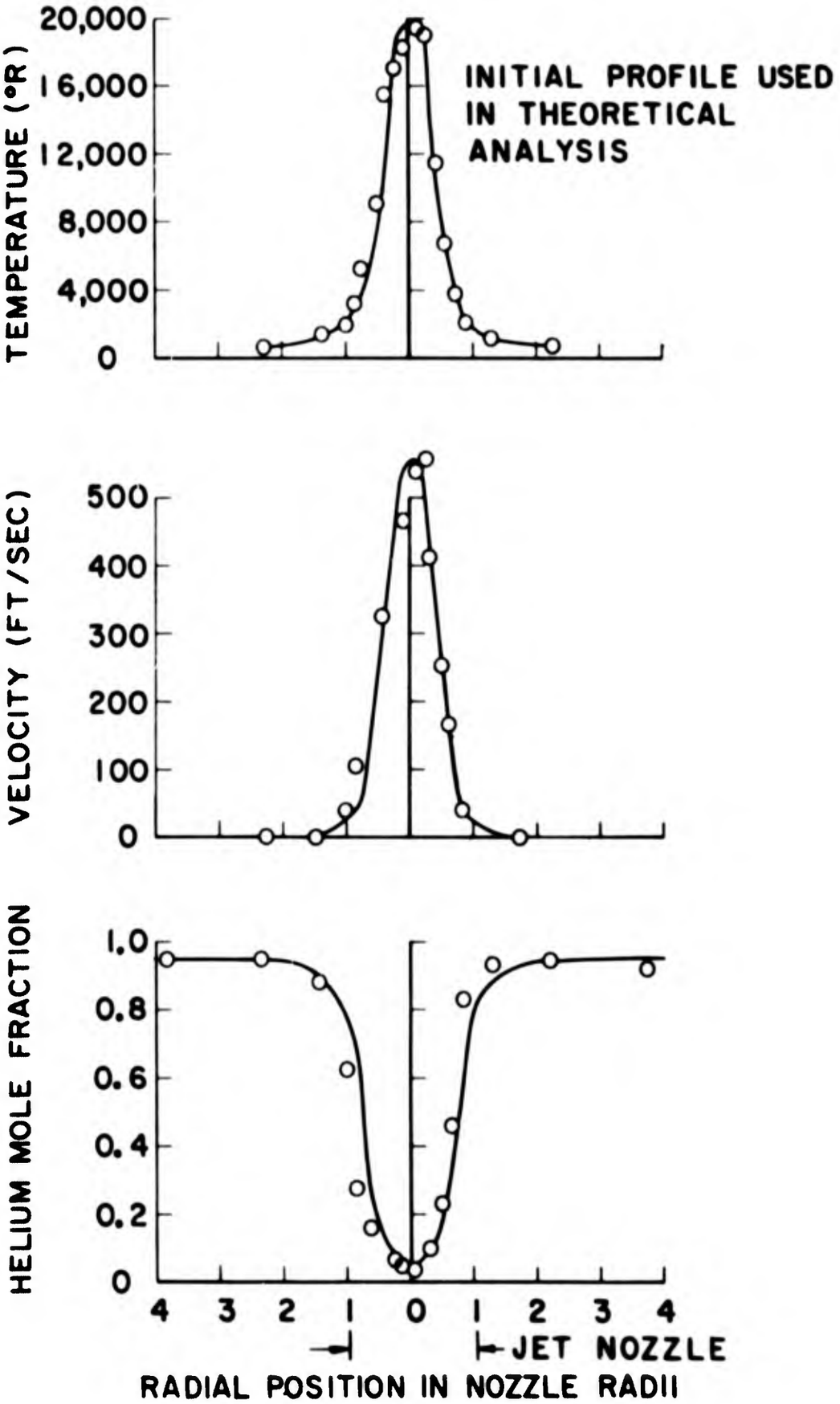

TEMPERATURE, VELOCITY, AND COMPOSITION PROFILES AT 1/32 INCH DOWNSTREAM FROM NOZZLE EXIT PLANE

FIGURE 9

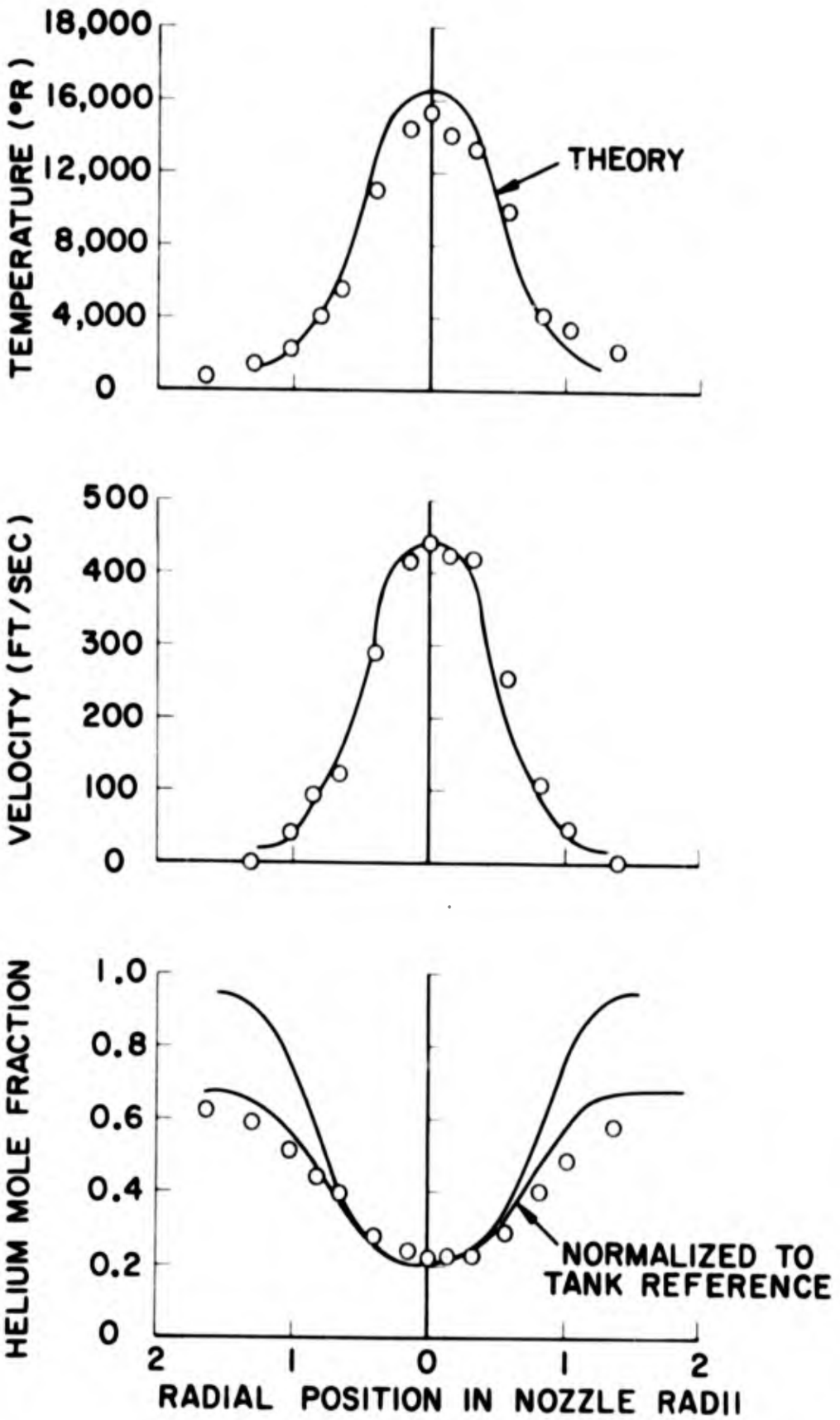

TEMPERATURE, VELOCITY, AND COMPOSITION PROFILES AT 5/16 INCH DOWNSTREAM FROM NOZZLE EXIT PLANE

FIGURE 10

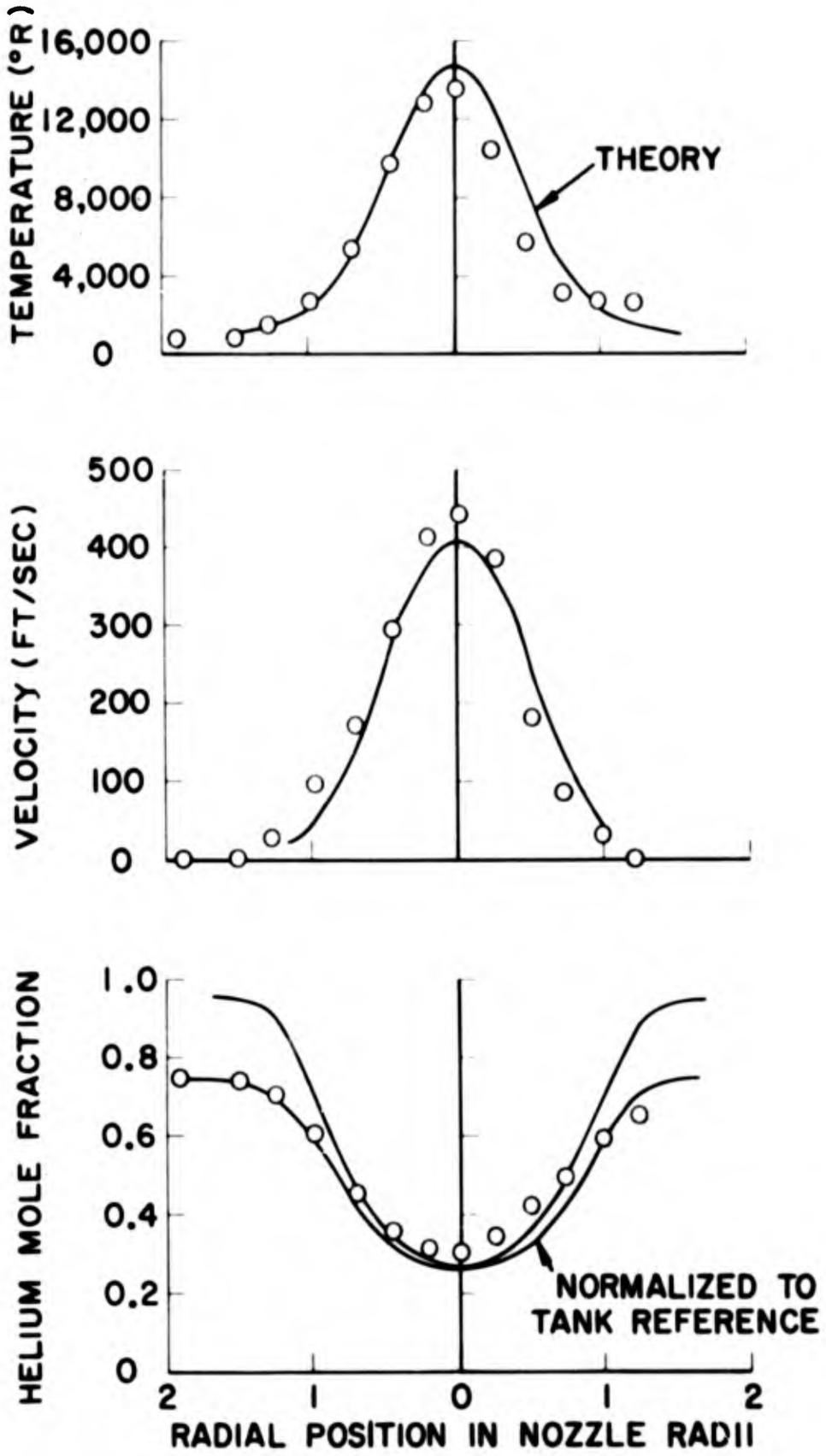

TEMPERATURE, VELOCITY, AND COMPOSITION PROFILES AT 1/2 INCH DOWNSTREAM FROM NOZZLE EXIT PLANE

FIGURE 11

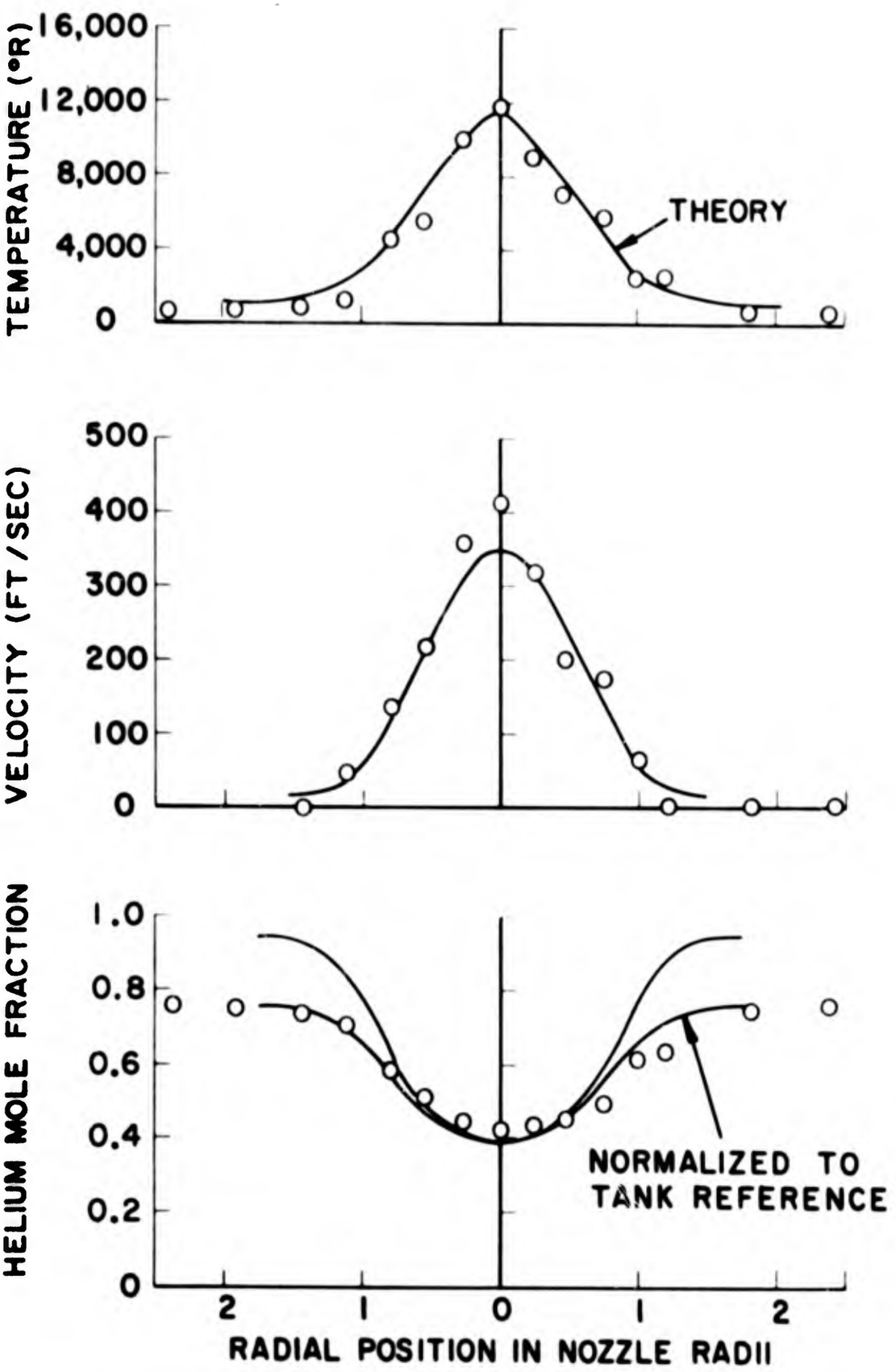

TEMPERATURE, VELOCITY, AND COMPOSITION PROFILES AT 1 INCH DOWNSTREAM FROM NOZZLE EXIT PLANE

FIGURE 12

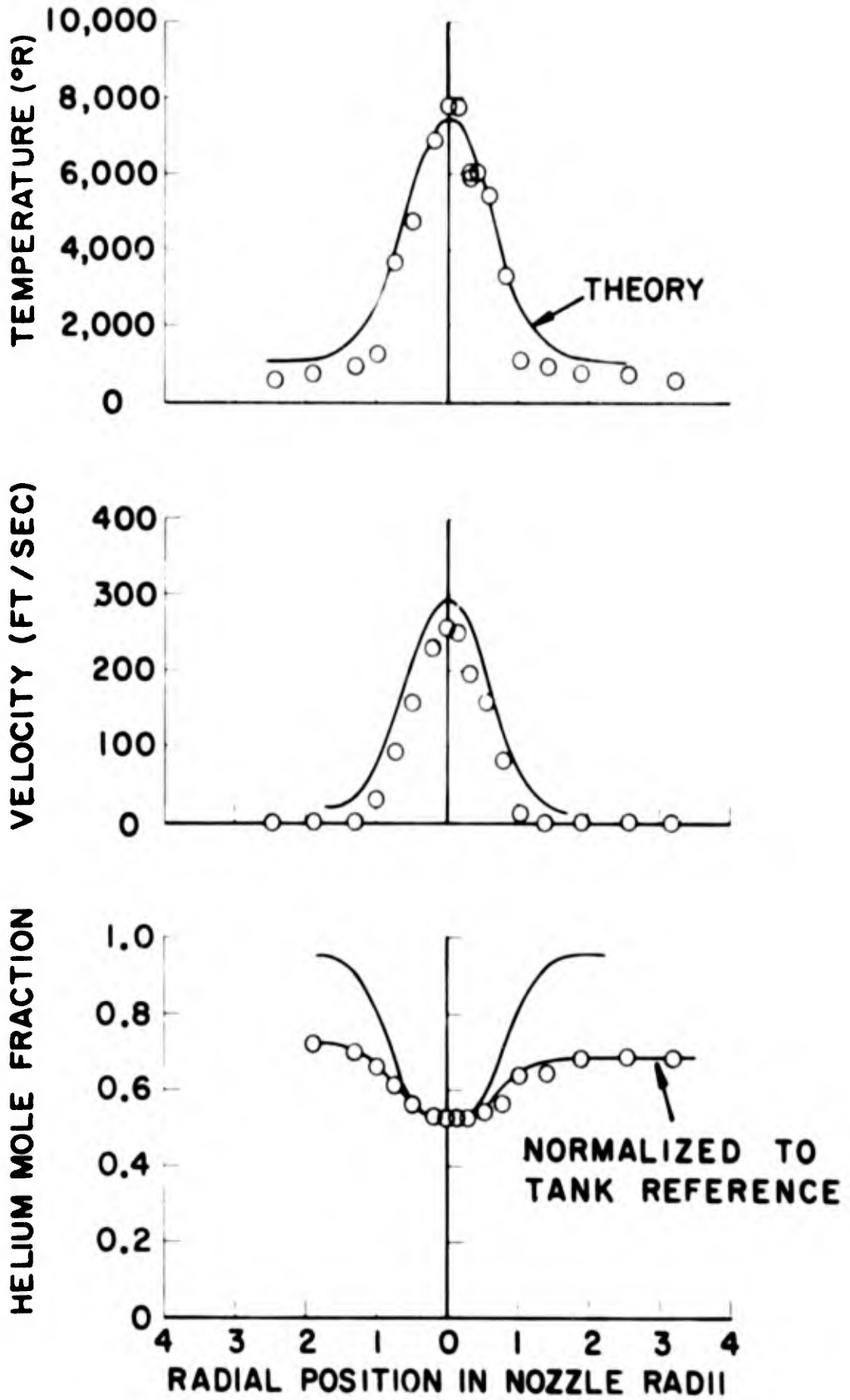

TEMPERATURE, VELOCITY, AND COMPOSITION PROFILES AT 2 INCHES DOWNSTREAM FROM NOZZLE EXIT PLANE

FIGURE 13

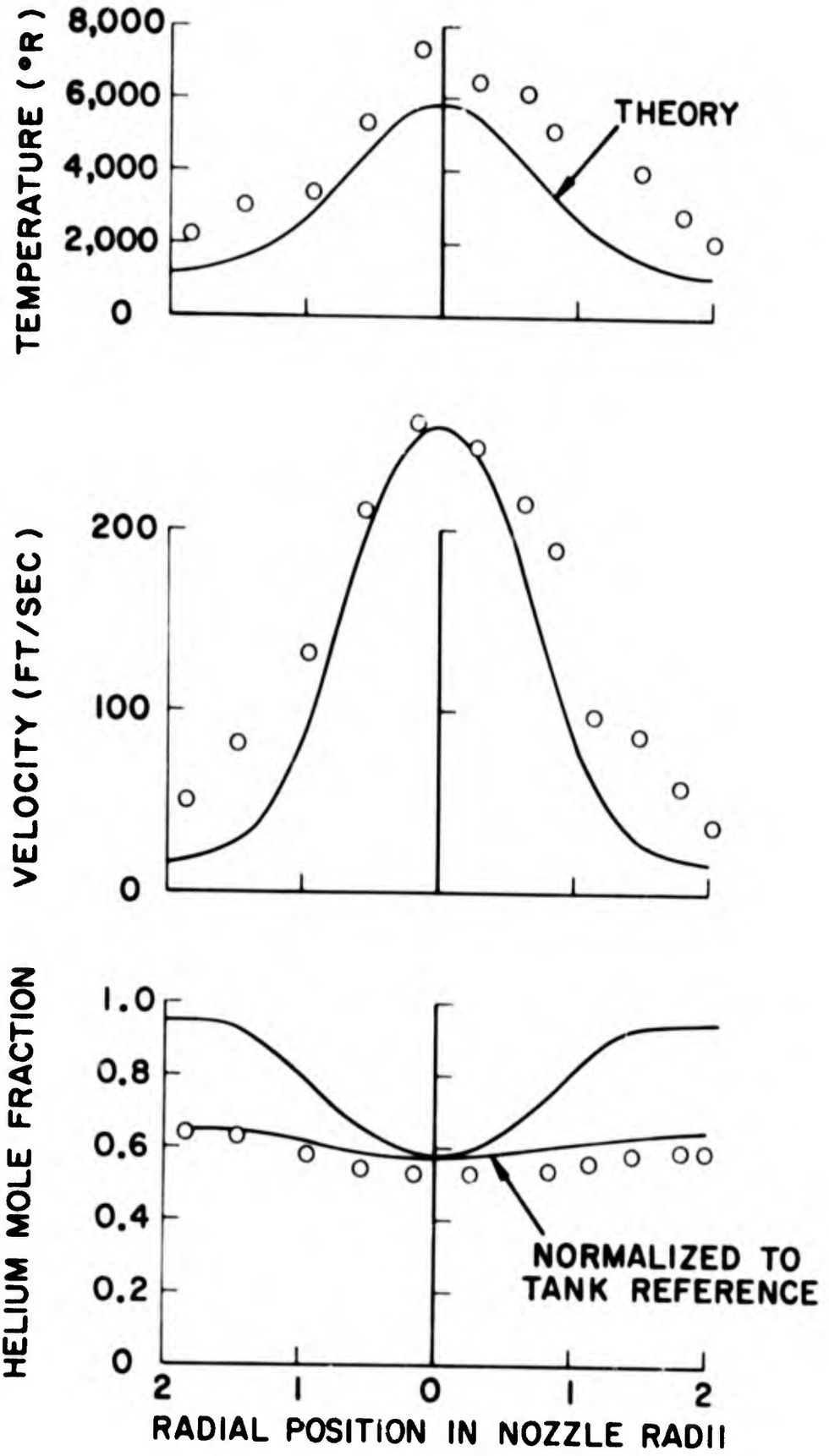

TEMPERATURE, VELOCITY, AND COMPOSITION PROFILES AT 3 INCHES DOWNSTREAM FROM NOZZLE EXIT PLANE

FIGURE 14

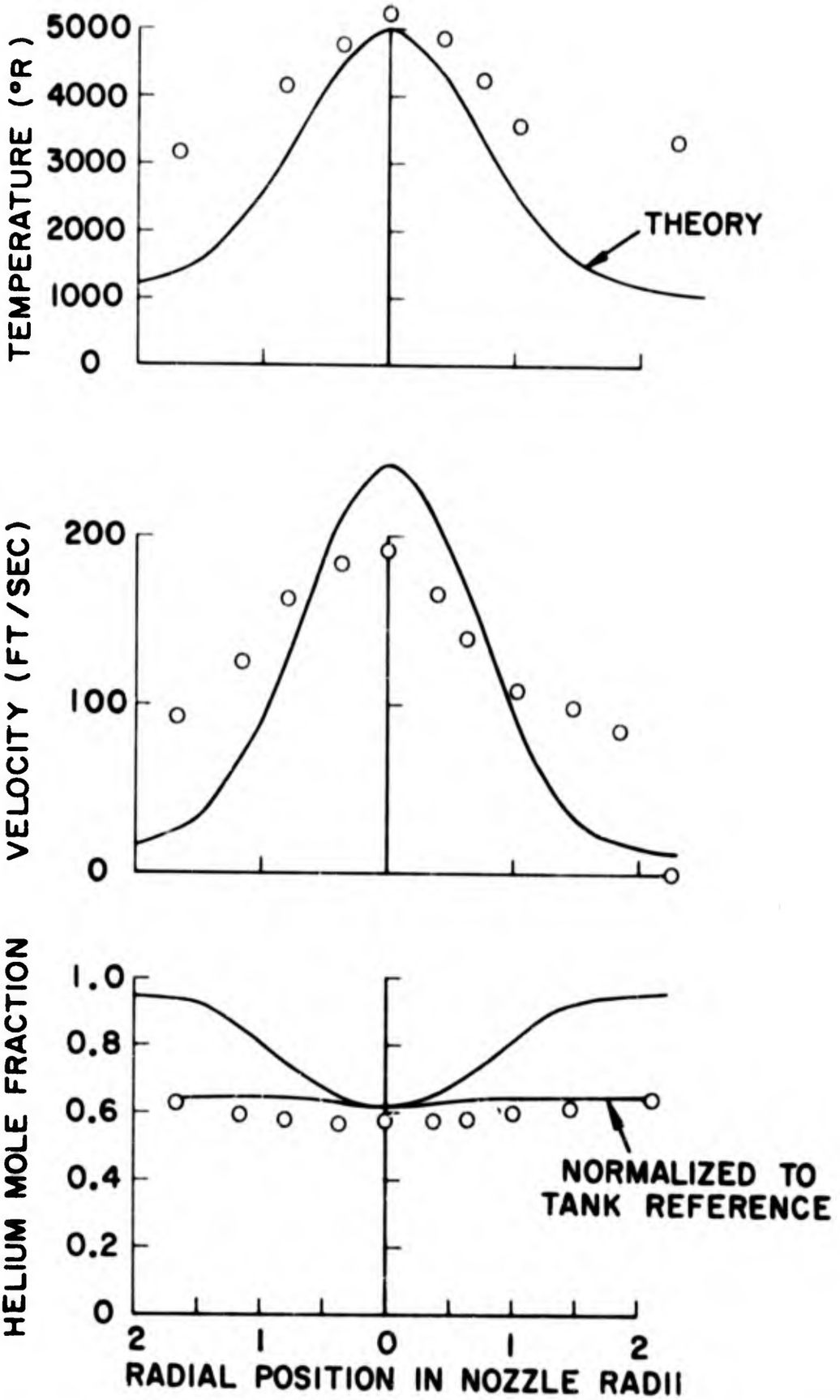

TEMPERATURE, VELOCITY, AND COMPOSITION PROFILES AT 4 INCHES DOWNSTREAM FROM NOZZLE EXIT PLANE

FIGURE 15

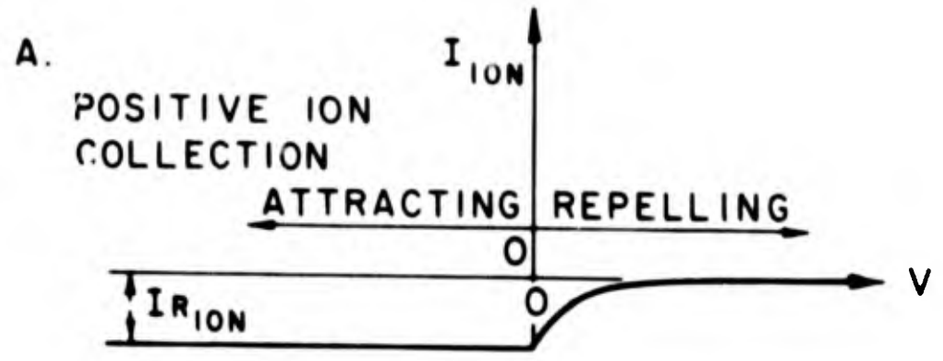

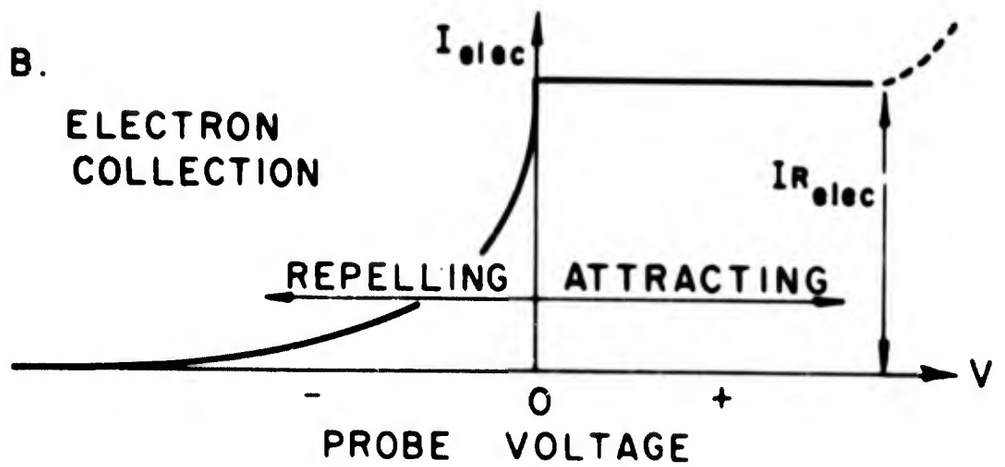

ILLUSTRATION OF ION AND ELECTRON CURRENTS AT ELECTROSTATIC PROBE SURFACE AS A FUNCTION OF PROBE POTENTIAL

FIGURE 16

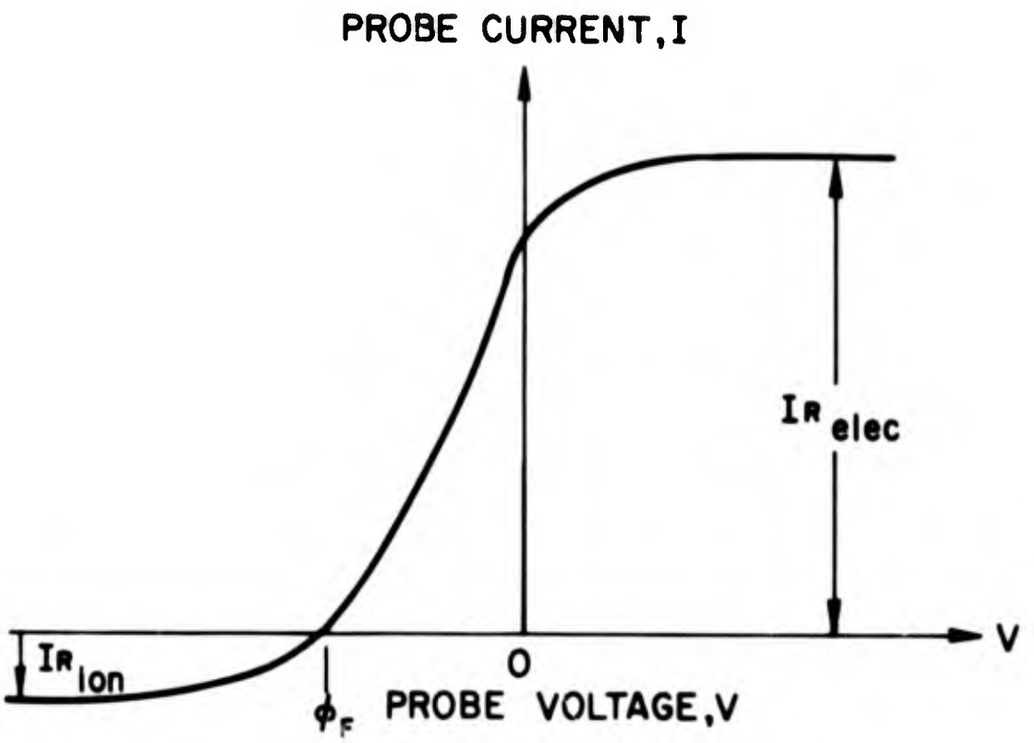

ILLUSTRATION OF A TYPICAL CURRENT-VOLTAGE CHARACTERISTIC FOR A LANGMUIR PROBE

FIGURE 17

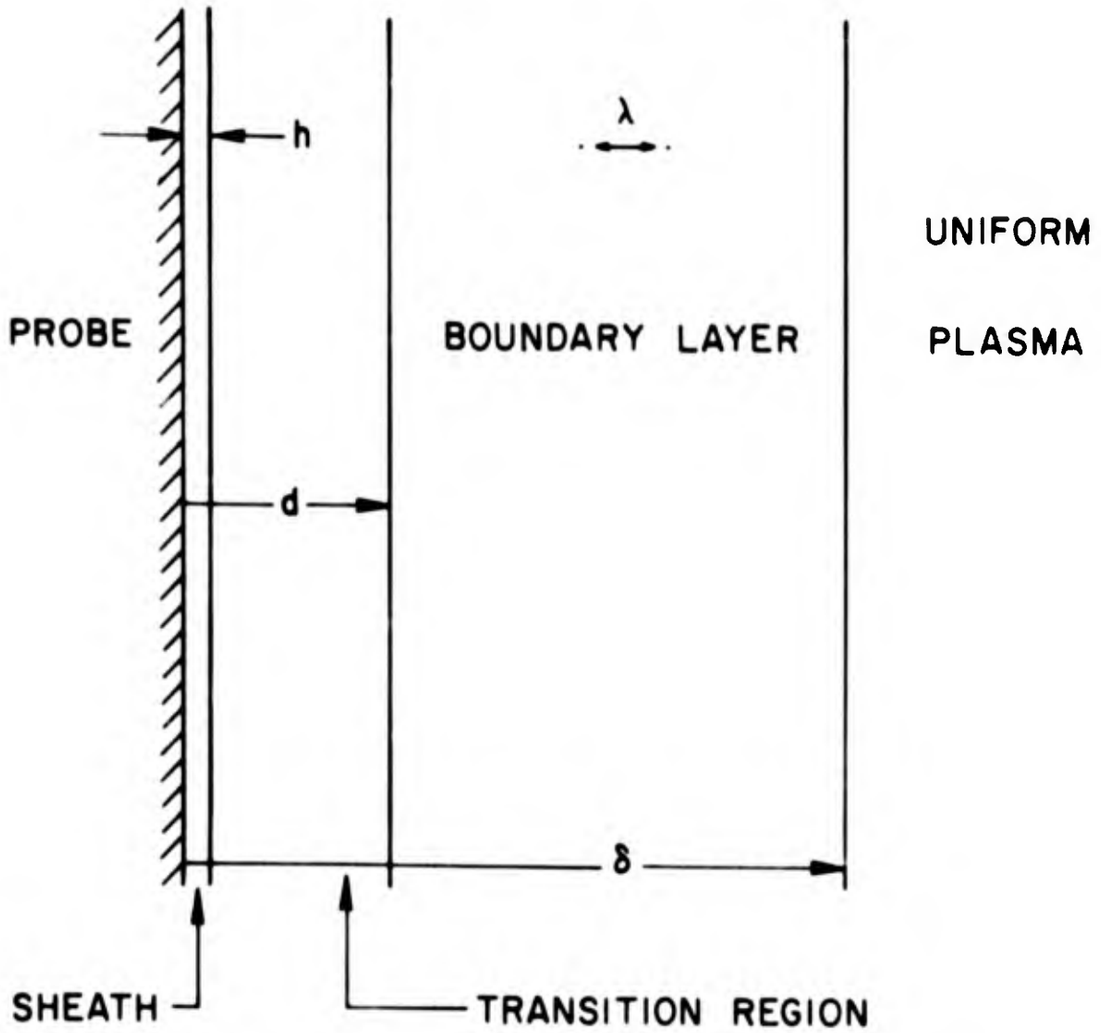

DEFINITION OF REGIONS NEAR AN ELECTROSTATIC PROBE

FIGURE 18

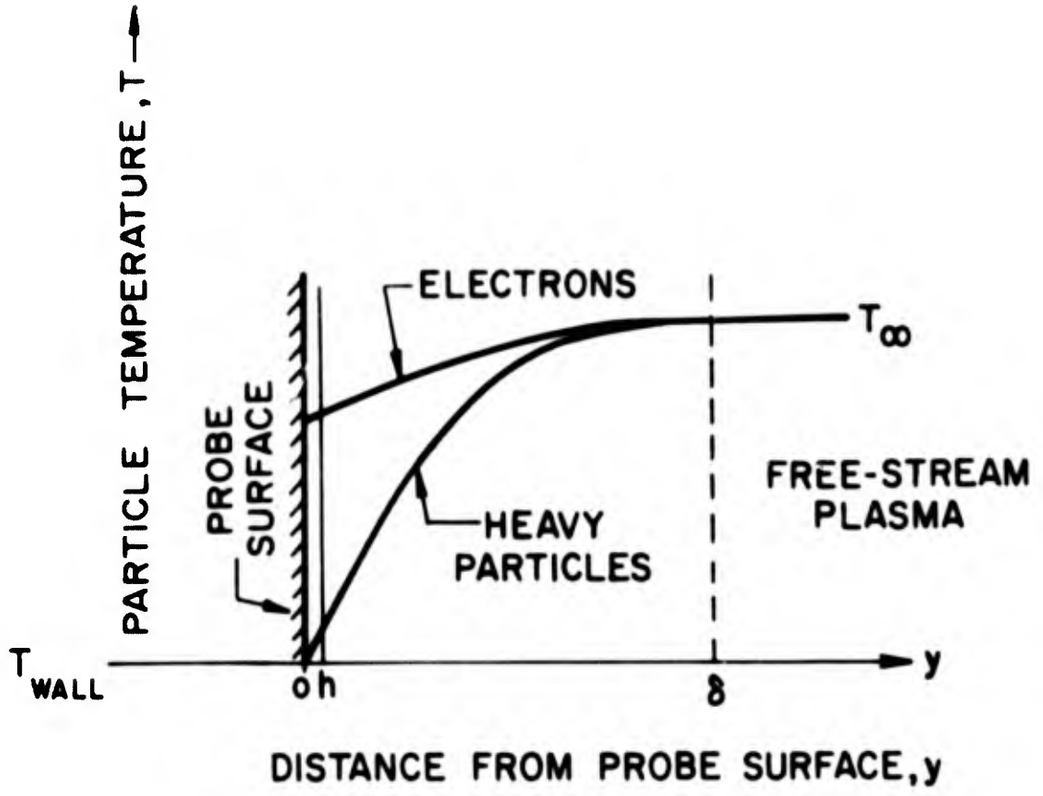

REPRESENTATION OF ASSUMPTIONS USED IN THE ELECTROSTATIC PROBE THEORY

FIGURE 19

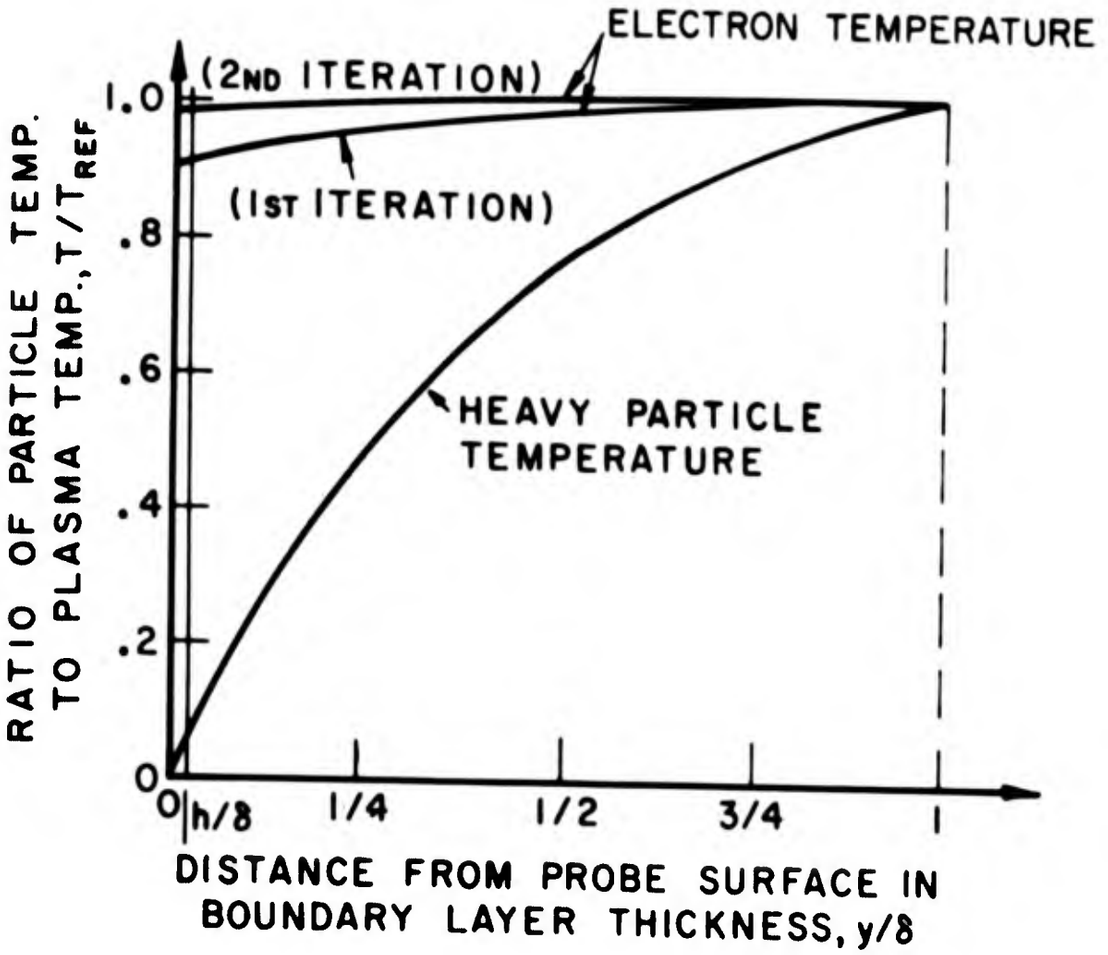

COMPUTED ELECTRON AND HEAVY PARTICLE TEMPERATURES NEAR AN ELECTROSTATIC PROBE

FIGURE 20

UNCALIBRATED ELECTROSTATIC PROBE DATA

FIGURE 21